NATIONAL ENERGY TECHNOLOGY LABORATORY

OIL & GAS

DOE Award No.: FP00003995

Final Project Scientific / Technical Report

PROPERTIES OF SEDIMENTS CONTAINING METHANE HYDRATE, WATER, AND GAS SUBJECTED TO CHANGING GAS COMPOSITIONS

Project Period (May 1, 2016 to September 30, 2018)

Submitted by:
Timothy J. Kneafsey

Signature

Lawrence Berkeley National Laboratory
DUNS #:xxxxxxx
1 Cyclotron Road
Berkeley CA 94720
Email: tjkneafsey@lbl.gov
Phone number: (510) 486-4414

Prepared for:
United States Department of Energy
National Energy Technology Laboratory

November 26, 2018

U.S. DEPARTMENT OF ENERGY | NATIONAL ENERGY TECHNOLOGY LABORATORY

Office of Fossil Energy

DISCLAIMER

Project Summary Report

LBNL-KIGAM Collaboration in the Investigation of the Gas Production Potential of Hydrate Deposits in the Korean East Sea

Submitted to the

Korea Institute of Geoscience and Mineral Resources (KIGAM)

and

National Energy Technology Laboratory (NETL)

by

Lawrence Berkeley National Laboratory (LBNL)

Energy Geosciences Division

1 Cyclotron Rd.

Berkeley, California 94720

USA

Principal Investigator: Timothy J. Kneafsey

Co-PI: George J. Moridis

Co-PI: Matthew T. Reagan

With contribution from Jihoon Kim (TAMU)

September 30, 2018

Executive Summary

This report summarizes activities carried out in the project entitled *LBNL-KIGAM Collaboration in the Investigation of the Gas Production Potential of Hydrate Deposits in the Korean East Sea.* Project performers include researchers at Lawrence Berkeley National Laboratory and Texas A&M University.

This report discusses two groups of tasks having the goal of improving understanding of the future production of methane from hydrate deposits in the Ulleung Basin (UB). The first group of tasks are numerical, performed using TOUGH+HYDRATE and other codes developed at Lawrence Berkeley National Laboratory. The second group of tasks are experimental, performed in laboratories at Lawrence Berkeley National Laboratory. All tasks were performed in collaboration with or with inputs from KIGAM.

Code Development and Simulation

To better simulate hydrate-related behavior relevant to testing and production of gas from the Ulleung Basin, the capabilities of the T+H/pT+H codes required enhancements through the additional of several non-Darcy flow effects. It is important to note that the new simulation capabilities leveraged recent NETL-funded work on coupled T-H-M simulation of shale gas and shale oil systems. Numerous enhancements were made to the TOUGH+HYDRATE code (T+H), and these have been described in a journal paper.

Using T+H+Millstone and the wellbore model, the LBNL team conducted simulations of gas productions and the associated geomechanical system response during gas production from hydrates at the Ulleung basin using the most recent geological model and the flow, and geomechanical properties provided by KIGAM researchers. These results have been submitted as a paper to *J. Pet. Sci. Eng*.

Our teammate at Texas A&M University successfully simulated the behavior of coupled flow and geomechanics at UBGH2-6. Considering more accurate axisymmetric formulation, the same conclusion as in the previous study - that the wellbore might not be stable, which can suffer from significant vertical slip – was obtained. Thus, careful consideration of geomechanics behavior is required. Currently, more simulation with various production scenarios and further in-depth analysis are ongoing to investigate geomechanical behavior such as subsidence, evolution of effective stress, and any potential of geological failure including wellbore collapse.

Laboratory studies

Two studies were performed to partially address the essential question: Can gas be effectively produced from the layered sand/mud system? These include studies of particle transport in sand/mud layered systems, and hydrate dissociation tests in

sand/mud systems at different rates to model different flows resulting from production methods and distance from the well.

In our studies under relevant effective stresses in the sand/mud and sand particle systems investigated, particle migration including kaolinite particles, diatoms, and micron-scale barite particles was not geomechanically significant. Geomechanical system failure was frequently observed when sand control was poor. Production of mud also occurred, but particle transport through the sand layer was minimal. The tests did not cover every foreseeable condition, however, and these results are in contrast with several other studies.

Table of Contents

Project Description

This report presents the results of five tasks performed to support investigation into the potential field test and gas production from layered sands and muds as found in the Ulleung Basin. Knowledge gained from this work will benefit KIGAM and USDOE in their consideration of natural gas production from suboceanic deposits containing methane hydrate. The five tasks include improvements to hydrate multiphase flow simulators that include geomechanical modeling, and simulations of test cases of interest. Laboratory tasks investigating the behavior of hydrate-bearing layered sand/mud systems, and particle transport in these systems were performed. The tasks are:

Task 1: Enhanced flow simulation capabilities for the simulation of complex mud/silt/sand hydrate-bearing systems

Subtask 1.1: Non-Darcy capabilities for T+H codes

Subtask 1.2: Simulation of complex mud/silt/sand deposits

Task 2: Enhanced geomechanical capabilities for the predictive simulation of potential UBGH field test sites

Task 3: Project Management, Communication, Reporting and Technology Transfer

Task 4: Gas production from a sand layer in a sand/mud layered system

Task 5: Mechanical and chemical behavior of diatomaceous medium and filtration behavior of sand

The work was performed over the time period of May 2017 to September 2018. Although originally the project was to start earlier, contracting and funding issues delayed the project start. Each task is presented individually below. Journal papers that were partially funded under this project are included as attachments, and not further summarized herein.

Task 1: Enhanced flow simulation capabilities for the simulation of complex mud/silt/sand hydrate-bearing systems

George Moridis, Matt Reagan

Subtask 1.1: Non-Darcy capabilities for T+H codes (LBNL portion - funded by US DOE)

Subtask 1.2: Simulation of complex mud/silt/sand deposits (funded by US DOE)

The TOUGH+HYDRATE code (T+H) received extensive physical properties upgrades, non-Darcy flow capabilities, and workflow enhancements.

T+H now includes several new physical properties relationships:

1. New water properties formulations (IAPWS, 2008 to 2014)
2. New gas viscosity estimation option: Friction theory (Quinones [2000])
3. New addition to the gas EOS options: Lee-Kessler (1975), new default for hydrocarbon gas enthalpy
4. New methods for computing hydrate thermophysical properties: Data-Gupta (2008); Ballard (2011)
5. New activity-based options to determine gas solubility in H_2O in addition to standard Henry's law
6. New capabilities to fully account for the effects of high salinity on hydrate formation

The T+H code has also been expanded by the inclusion of non-Darcy flow capabilities, including turbulent flow and gas-slippage effects (when effective permeabilities are below the micro-Darcy level) covering the spectrum from Klinkenberg flow to Knudsen diffusion (Malek et al., 2003). The drift-flux model (Shi et al., 2005) has been incorporated into the code for the simulation of coupled wellbore interactions, and Forchheimer flow has been added to handle high fluid velocities in high-permeability media (Barree, and Conway, 2004).

Workflow enhancements to the code include time-variable boundary conditions, monitoring of 3D regions of varying shapes, monitoring of flow through user-defined 2D and 3D interfaces, and new output formats (conversion to VTK and silo files).

The latest version of T+H was released in January 2018 and documented in the following paper:

Moridis, G.J., Queiruga, A.F., Reagan, M.T., "The T+H+M Code for the Analysis of Coupled Flow, Thermal, Chemical and Geomechanical Processes in Hydrate-Bearing Geologic Media," *Proc.* 9th Int. Conference on Gas Hydrates, Denver, CO, 1-3 June 2017.

We have also completed development of the latest T+M simulator by coupling the latest T+H simulator to Millstone, a new geomechanical code that offers new

abilities and fixes many computational and mathematical shortcomings of earlier codes used to describe the geomechanical response of hydrate-bearing systems. The new formulation includes the ability to perform geomechanical simulations with 2D radially symmetric meshes to represent 3D vertical well problem, increasing numerical efficiency.

The new T+H/Millstone platform is described in a recently submitted paper:

Moridis, G.J., Reagan, M.T., Queiruga, A.F., "The TOUGH+Millstone Code for the Analysis of Coupled Flow, Thermal, Chemical and Geomechanical Processes in Hydrate-Bearing Geologic Media, Part I: The Hydrate Simulator," submitted to *Transport in Porous Media*.

Using T+H+Millstone and the wellbore model, the LBNL team has been conducting simulation of gas productions of the associated geomechanical system response during gas production from hydrates at the Ulleung basin using the most recent geological model and the flow and geomechanical properties provided by KIGAM researchers. The coupled Millstone code allows for separate flow and mechanics meshes, resulting in greater numerical efficiency (Figure 1.1). The simulations considered large-deformation geomechanics (not fully considered in earlier studies) and plasticity. The new, more efficient formulation of Millstone, which uses an axisymmetric/cylindrical 2D model instead of a 3D wedge, is substantially more physically and numerically accurate in describing the near-well region around a vertical well and also computationally more efficient. Thus, some earlier simulations were re-run using the new code.

.

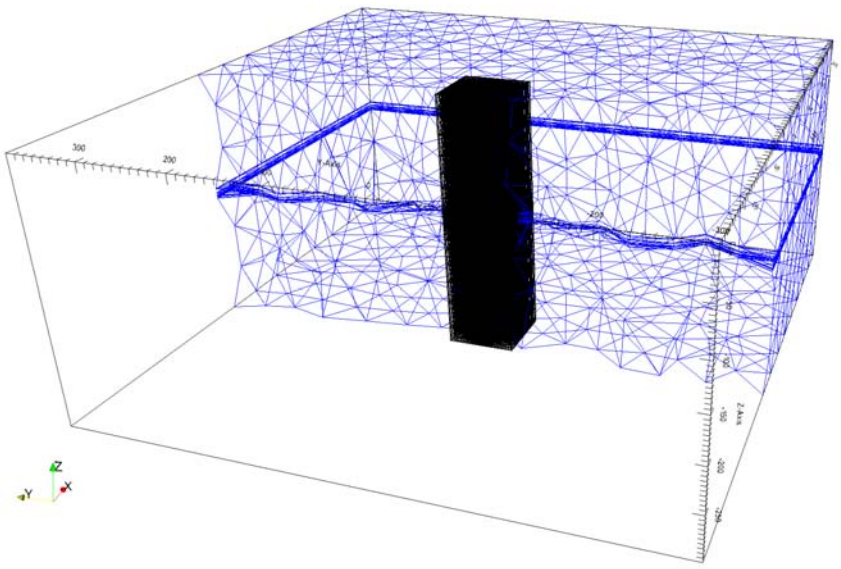

Figure 1.1. Domain of the flow problem as a TOUGH+ mesh domain (black, centered) inset in a larger geomechanical domain with a finite element mesh solved by Millstone (blue, cut halfway with extent outlined).

In addition, using a new post-processing capability for coupling flow and geomechanics, we revisited earlier simulations (documented in a 2016 report) and performed a 1-way coupling of the 2016 production simulation results to the new Millstone geomechanical simulator using the tough-convert analysis package.

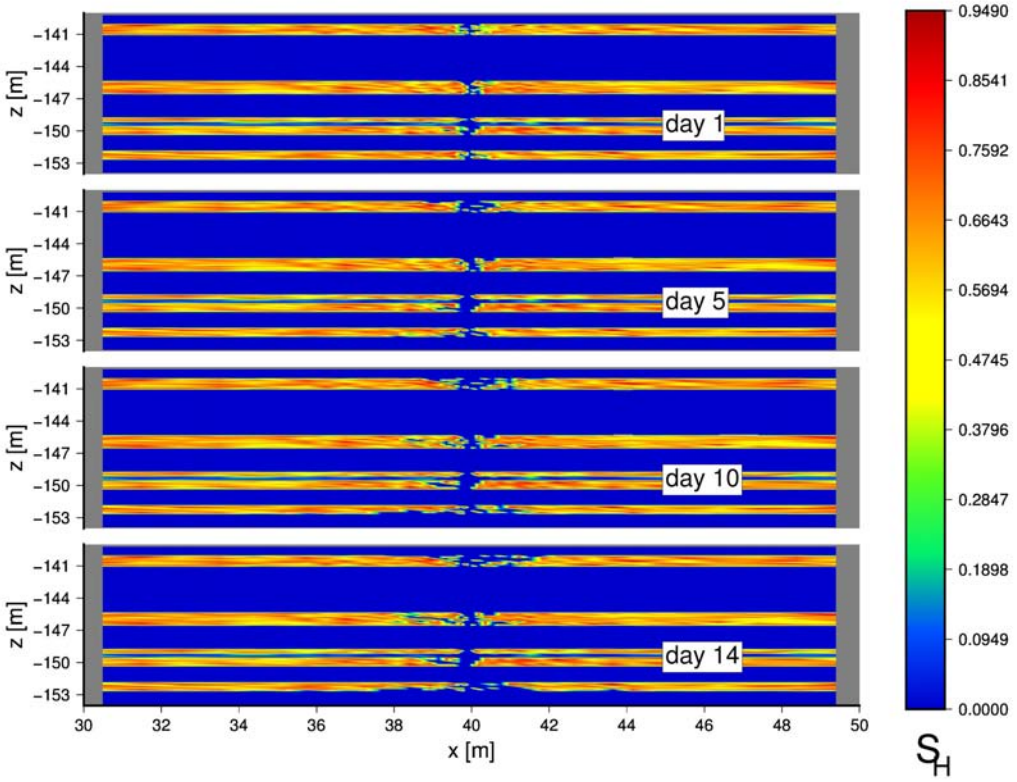

Figure 1.2. Case kϕS: Hydrate saturation (S_H) distributions on the x-z plane at y = 40 m during the 14-day long production test (P_w = 9 MPa).

The simulation results show that:

1. The gas release and production rates are generally low and the affected region of the reservoir is limited (Figure 1.2).
2. The water production accompanying gas production from this deposit appears manageable (in terms of absolute rates and volumes) under all the scenarios investigated in this study; however, in relative terms the water-to-gas ratio is very high during the 14-day production test and stabilizes relatively early.
3. The maximum subsidence at the seafloor is predicted to be 0.016m, but the maximum subsidence and uplift of the top and bottom of the reservoir, respectively, is predicted to have a magnitude of 0.22m (Figure 1.3).
4. Reservoir heterogeneity decreases the magnitude of the geomechanical response.

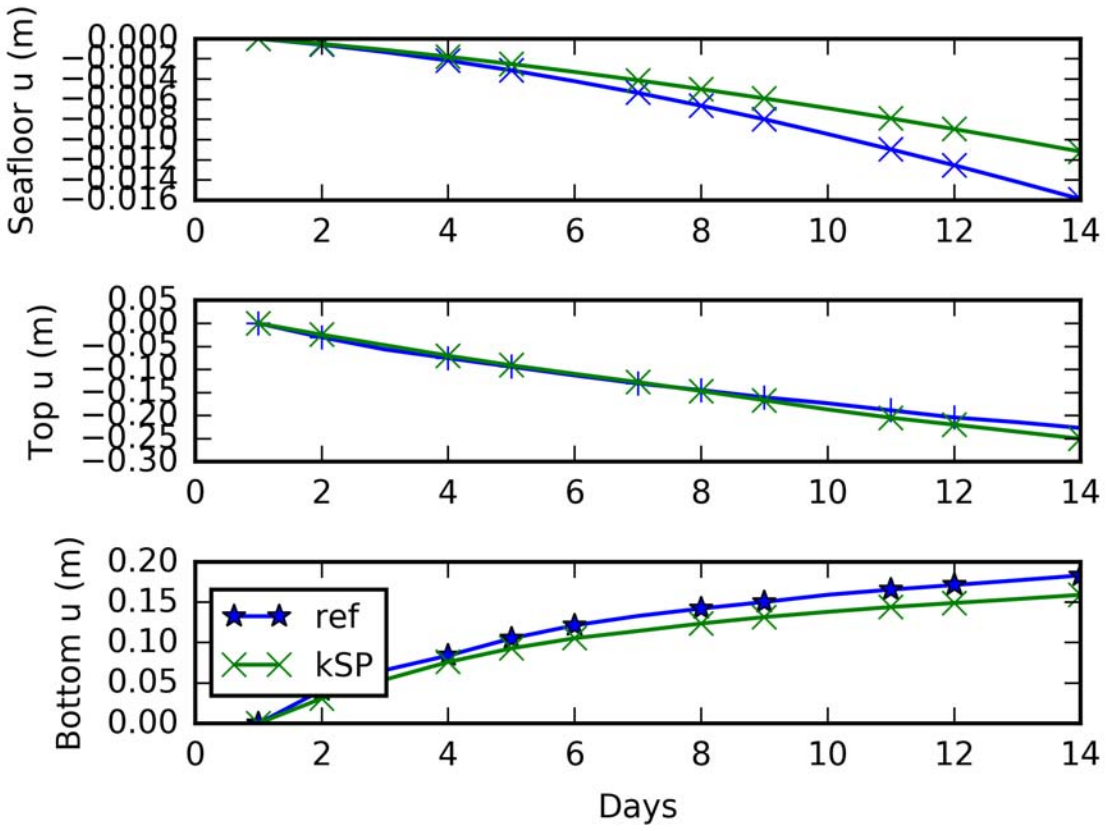

Figure 1.3: Vertical displacement history of the system of both cases at the seafloor (z = 0 m), top of the reservoir (z = -140 m), and bottom of the reservoir (z = -153 m).

The new results were submitted as a paper to *J. Pet. Sci. Eng.*:

Moridis, G.J., Reagan, M.T., Queiruga, A.F., Kim, S.-J. "System Response to Gas Production from a Heterogeneous Hydrate Accumulation at the UBGH2-6 Site in the Ulleung Basin of the Korean East Sea," in press, J. Pet. Sci. Eng.

Task 2: Enhanced geomechanical capabilities for the predictive simulation of potential UBGH field test sites (funded by KIGAM)

Jihoon Kim (Texas A&M University)

Numerical investigation of depressurization and gas production at UBGH2-6: Coupled flow-geomechanics simulation

Introduction

We employ the axisymmetric domain of simulation, considering gas production with a vertical well. In the previous study, the geomechanics domain did not fully follow the formulation of axisymmetric geomechanics. In other words, we used the *Cartesian coordinate system* for the geomechanics problem, which FLAC3D only allows, where the geomechanics domain was like a slice of a pie. As a result, inaccuracy near the well area might exist. In this study, we take the exact formulation of axisymmetric geomechanics in order to have more accurate results. Precisely, we take the *cylindrical coordinate system* of stress and momentum balance to calculate deformation and stress near the wellbore appropriately. Also, we use an in-house simulator of coupled flow and geomechanics (TOUGH+Hydrate-ROCMECH), while T-F (TOUGH+Hydrate-FLAC3D) was used in the previous study.

From numerical results, for long production of depressurization, we identify small subsidence at the surface but significant vertical displacement above the hydrate zones. Thus, as found in the previous study, careful consideration for wellbore stability is required.

Numerical simulation

The site of UBGH2-6 is located near the sea floor in the East Sea, South Korea, having significant overburden in the deep sea (Figure 2.1). The hydrate zone consists of alternating hydrate-bearing sand and mud layers. As shown in the right of Figure 2.1, we take the domain of 250m by 220m for numerical simulation, which has irregular sizes of grid blocks (160 by 140). In particular, we have small gridblocks near the vertical well and the hydrate zone.

The initial pressures at the top and bottom are 23.1MPa and 24.59MPa, respectively, and the initial temperatures at the top and bottom are 6.366 ^{o}C and 18.633 ^{o}C, respectively. They are distributed linearly from top to bottom. The initial hydrate saturation in the hydrate zone is 0.65, while it is zero in the other zones. The initial vertical and horizontal stresses are -23.1MPa and -3.47 MPa, respectively, and they are distributed vertically with the gradients of -25.0kPa and -3.47 kPa. Tensile stress is positive. Table 2.1 shows the main properties of flow and geomechanics simulation. We produce gas by depressurization, applying the constant bottom hole pressure of 9MPa.

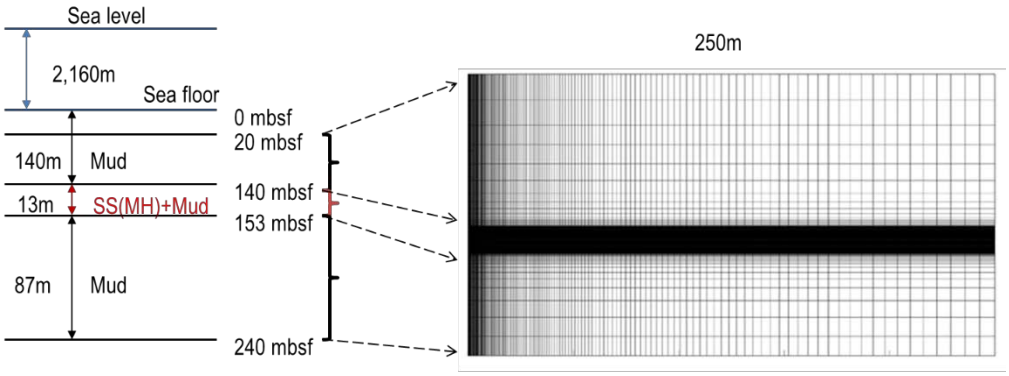

Figure 2.1 Left: geological information of UBGH2-6 Right: discretized domain for flow

Table 2.1. Material properties for flow and geomechanics

Property	Overburden	Hydrate layer	Mud-Interlayer	Underburden
Drained bulk modulus, SH=0%	15.55 MPa	27 MPa	20 MPa	22 MPa
Drained shear modulus, SH=0%	5.185 MPa	16 MPa	6.667 MPa	7.407 MPa
Drained bulk modulus, SH=100%	285 MPa	933.33 MPa	285 MPa	285 MPa
Drained shear modulus, SH=100%	99.75 MPa	560 MPa	99.75 MPa	99.75 MPa
Permeability, SH=0%	0.02 mD	500 mD	0.14mD	0.02 mD
Initial porosity	0.76	0.45	0.67	0.0

Figs. 2.2 and 2.3 show distributions of pressure, gas saturation, temperature, and hydrate saturation after 14day and 100day productions, respectively. Depressurization induces dissociation of gas hydrates, which produces gas, shown in

Figs. 2.2 and 2.3 (a), (b), and (d). Also, dissociation of gas hydrate is endothermic reaction, and thus temperature decreases (Figs. 2.2 and 2.3(c)).

In Figure 2.4, we identify changes in pressure, gas and hydrate saturations at the two different monitoring points (mud and sand layers, respectively) near the wellbore. Pressure drops fast (Figure 2.4 (a)), which can dissociate gas hydrate (Figure 2.4 (d)), and thus gas is produced (Figure 2.4 (b)). Also, from Figure 2.4 (c), we find small vertical displacement away from the well at the hydrate zone.

However, as shown in Figure 2.5, significant vertical displacement can be found near the well and above the hydrate zone after 100 days, where the vertical displacement ranges up to 1m, although the vertical displacement after 14 days at the same location is about 0.3m. On the other hand, the surface subsidence does not look critical, having the vertical displacement of 0.05m after 100 days and -0.02m (uplift) after 14 days. Figure 2.6 shows distribution of volumetric strain after 100days. We identify significant compaction near the wellbore (particularly just above the perforation area).

Figs. 2.7-2.9 show the distributions of effective stress after 100 days. The changes of effective stress correspond to the depressurized area. Specifically, the compressive volumetric mean effective stress shown in Figure 2.9 induces large compaction in Figure 2.6, followed by the aforementioned substantial vertical displacement.

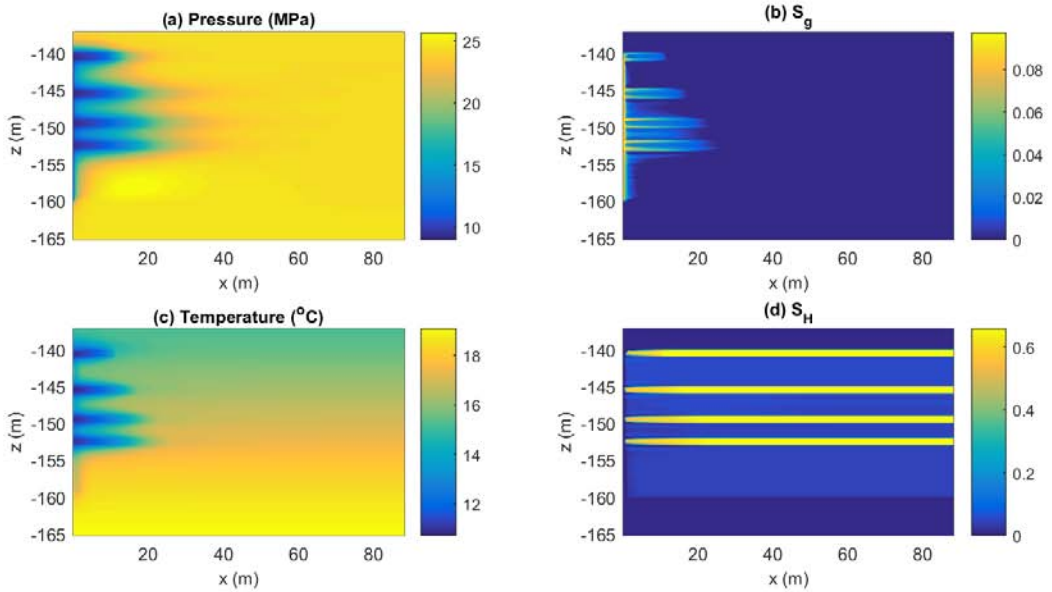

Figure 2.2 Distributions of pressure (a), gas saturation (b), temperature (c), and hydrate saturation (d) after 14 day production.

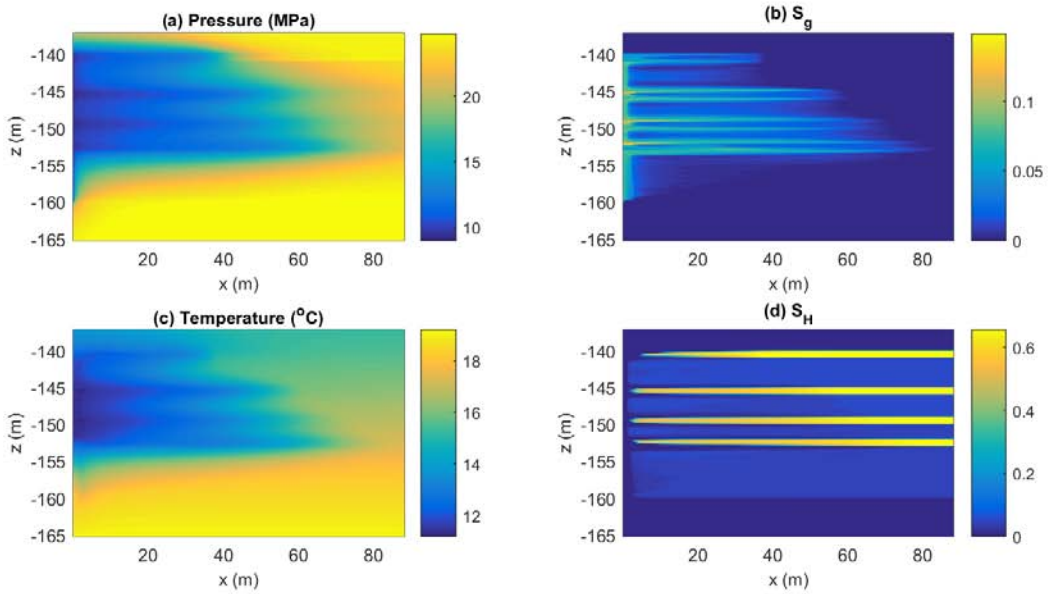

Figure 2.3 Distributions of pressure (a), gas saturation (b), temperature (c), and hydrate saturation (d) after 100 day production.

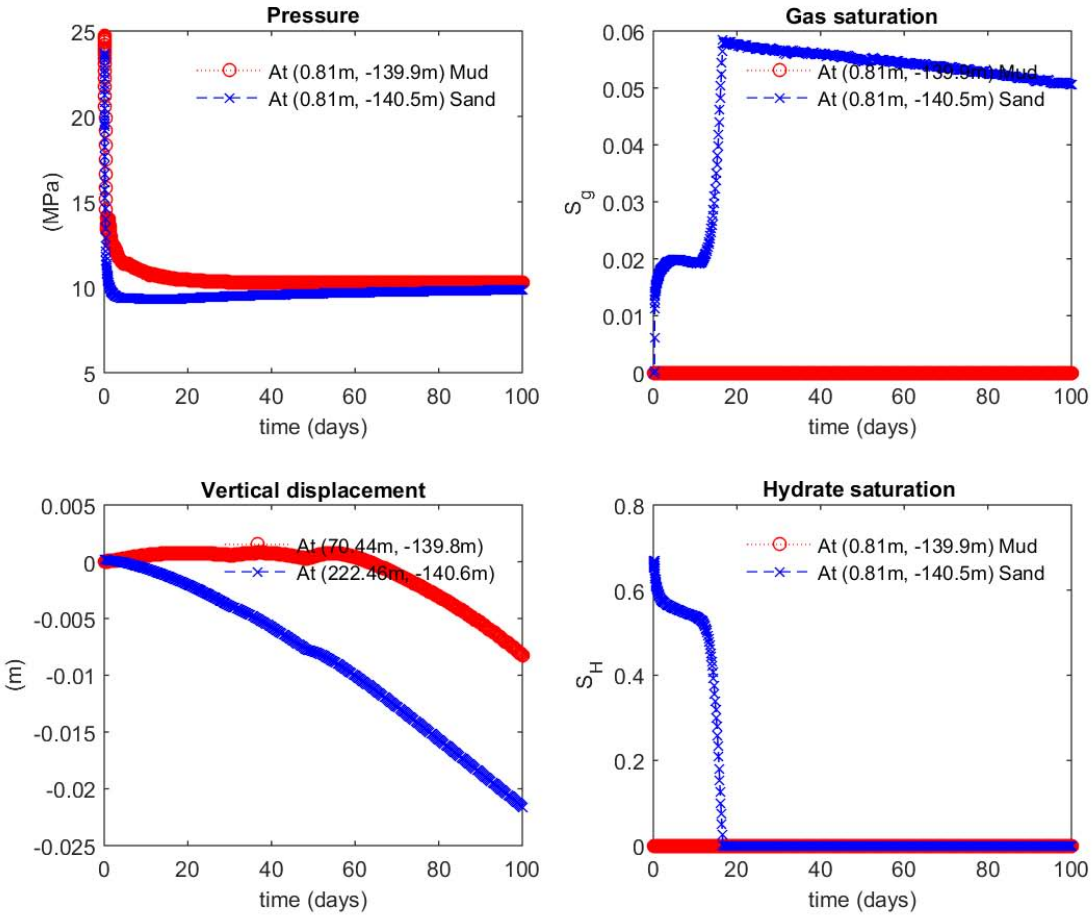

Figure 2.4. Evolutions of pressure (a), gas saturation (b), vertical displacement (c), and hydrate saturation (d) at two different locations.

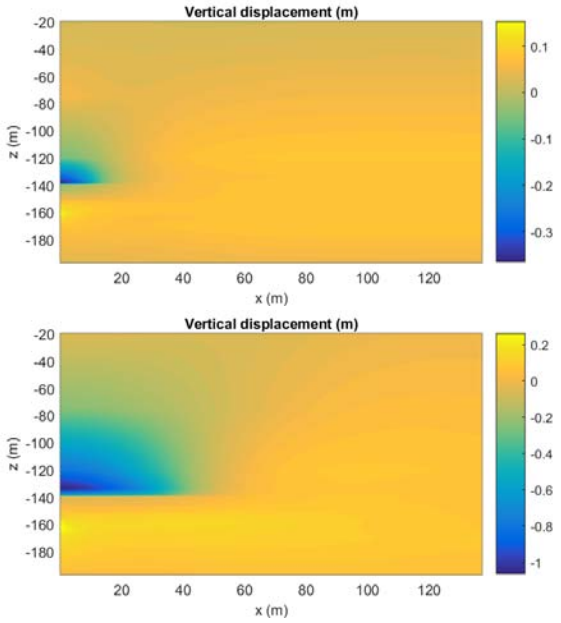

Figure 2.5 Distribution of vertical displacement. Left: 14 day production. Right: 100 day production.

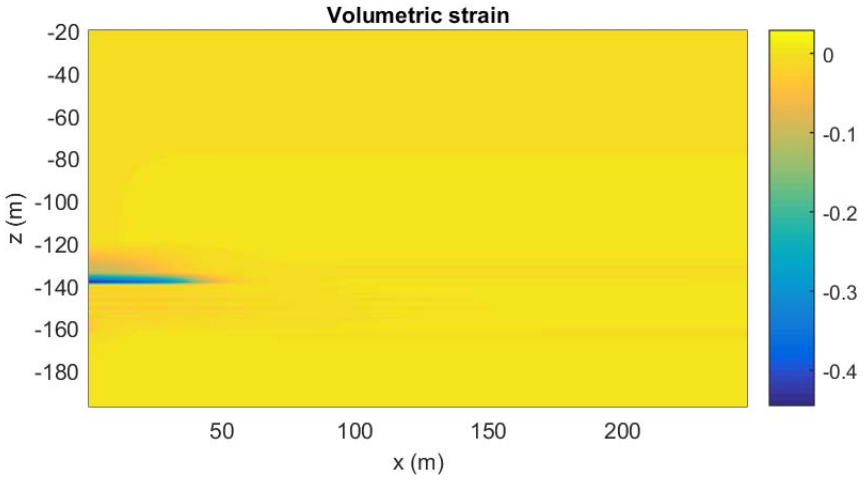

Figure 2.6 Distribution of volumetric strain (ε_v) after 100 days.

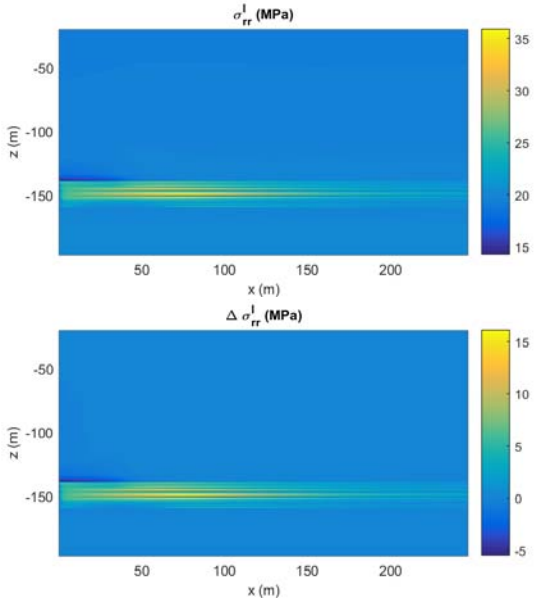

Figure 2.7 Left: Distribution of radial effective stress (σ'_{rr}) after 100 days. Right: Distribution of change of radial effective stress ($\mathbf{\Delta}\sigma'_{rr}$) from the initial state after 100 days.

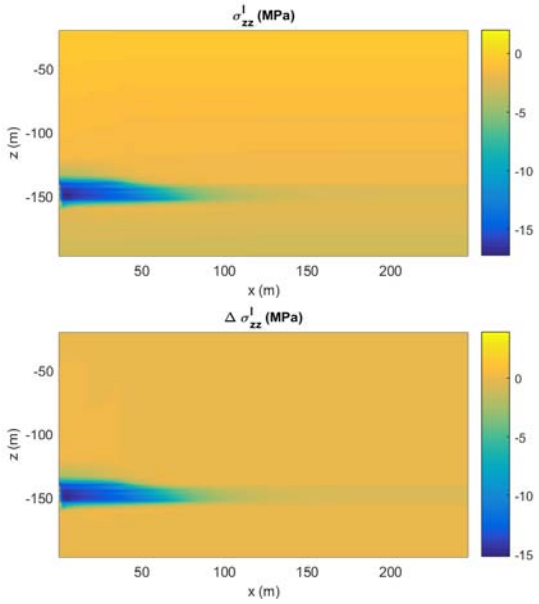

Figure 2.8 Left: Distribution of vertical effective stress (σ'_{zz}) after 100 days. Right: Distribution of change of vertical effective stress ($\mathbf{\Delta}\sigma'_{zz}$) from the initial state after 100 days.

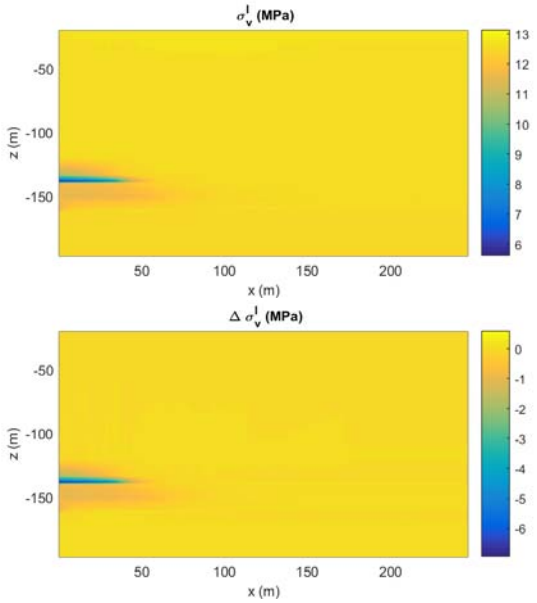

Figure 2.9 Left: Distribution of volumetric mean effective stress (σ'_v) after 100 days. Right: Distribution of change of volumetric mean effective stress ($\mathbf{\Delta}\sigma'_v$) from the initial state after 100 days.

Summary

We have successfully simulated the behavior of coupled flow and geomechanics at UBGH2-6. Considering more accurate axisymmetric formulation, we obtained the same conclusion in the previous study that the wellbore might not be stable, which can suffer from significant vertical slip. Thus, careful consideration of geomechanics behavior is required. Currently, more simulations with various production scenarios and further in-depth analysis are ongoing to investigate geomechanical behavior such as subsidence, evolution of effective stress, and any potential of geological failure including wellbore collapse.

Task 3: Project Management, Communication, Reporting and Technology Transfer (funded by US DOE)

This task supported project coordination between LBNL, NETL, KIGAM, and TAMU, and reports.

Task 4: Gas production from a sand layer in a sand/mud layered system
Tim Kneafsey, Sharon Borglin, Bin Wang

Duration: 12 months, i.e., from 5/16/2017 to 4/13/2018
Budget: $70K (LBNL portion – funded by KIGAM)

The essential question in this task is can gas be effectively produced from the layered sand/mud system. To investigate this, layered sand/mud systems were constructed in a laboratory pressure vessel using simulated media. The media in the mud layer consisted of a mixture of silt (200g), kaolinite (50g) diatomaceous earth (2.5g) and water (50g), based roughly on mud composition reported in the Ulleung basin (Kim et al, 2013). Barium sulfate was also added to the mud layer enhance contrast (1g). F110 sand with 30% saturation was used for the sand layer. Both layers were packed in half cylinder molds and frozen to aid the packing process (see Figure 4.1) in a method similar the one used to study mud erosion by Oyama et al, 2016. The resulting sample was 2 inches in diameter and 6 inches long, was placed in a EDPM sleeve with an inner diameter of 2 inch and length 8 inches. Endcaps were added to the system and the sample assembly was placed in an aluminum pressure vessel. The vessel is equipped with temperature sensors in the inlet and outlet and confining fluid and sensors for monitoring pressure inlet, outlet and confining fluid. Confining fluid consisted of a 1:1 water to propylene glycol mixture. The pressure, volume, and flow rates of the confining, upstream, and downstream Isco syringe pumps were also measured and recorded. Not shown in Figure 4.1 is a widening of the outlet flow to a sediment trap which was installed to monitor movement of sand and fines.

Figure 4.2 shows the packed mud/sand layered sample before and after pressurization. The mud layer is on top and sand layer on bottom. As the figure shows, after the confining pressure was applied, the sample compressed causing deformation due to the different compressibilities of the mud and sand. In this test the outlet tube was located mid sample and plugged with nylon mesh.

Methane hydrate was formed in the sample using the excess gas method at constant pore pressure (700 psi) and confining pressure (820 psi) at 3.5 °C. Literature search on conditions in the Ulleung Basin were conducted and it was concluded that 100 to 400 psi is a realistic range of effective stress related to production (Yun et al, 2010; Kim et al, 2013; Lee et al, 2011). After hydrate formation, the sample was saturated by pulling water through the sample with a downstream pump at a rate of 0.5 mL/min while maintaining the upstream pump at constant pressure.

Two hydrate experiments are described below, one in which the hydrate was dissociated with a slow depressurization, the other with a faster pressure decrease. For slow depressurization, pore pressure was reduced stepwise from 700 psi to 550

psi over 1.25 hrs, while in the fast depressurization test pore pressure was dropped from 700 psi to 500 psi over 10 min. In the slow depressurization test, prior to dissociation and after hydrate equilibration, water and CH_4 were allowed to flow through the system to observe any geomechanical changes or fines migration. Both tests were constructed similarly, however in the rapid depressurization test the outlet was located mid sample and was screened with nylon material, as depicted in Figure 4.1, and no flow of gas or water was performed. In the slow depressurization test the outlet was located at the end of the sample, and sand migration was prevented by an aluminum screen (mesh size 0.011 inch). In both tests hydrate formation, dissociation and any sample deformation were observed using the X-ray CT imaging.

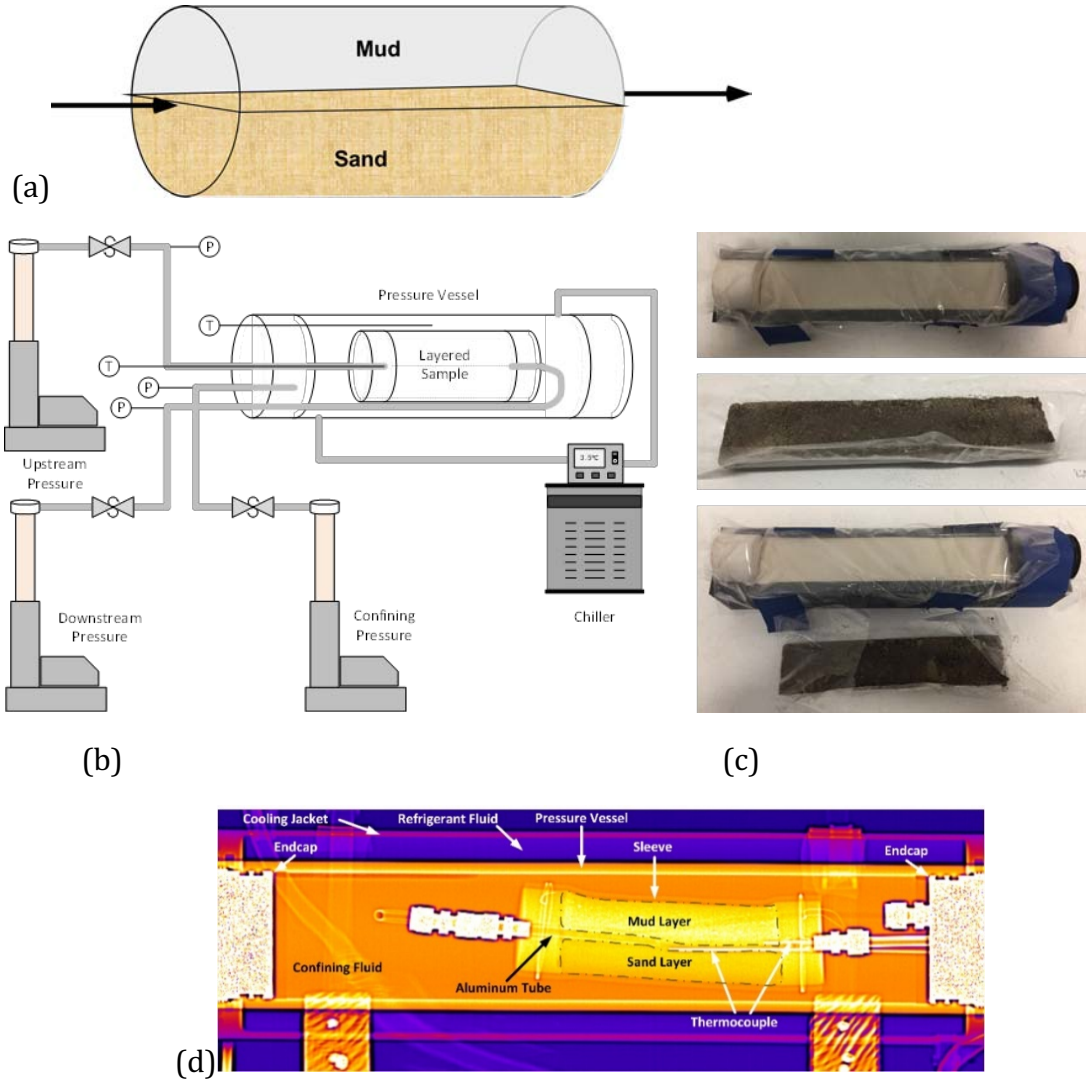

Figure 4.1. (a) Gas production test schematic. (b) schematic diagram of the experimental setup, (c) packed mud/sand layer in molds prior to sample packing, and (d) CT image of packed sample after pressurization.

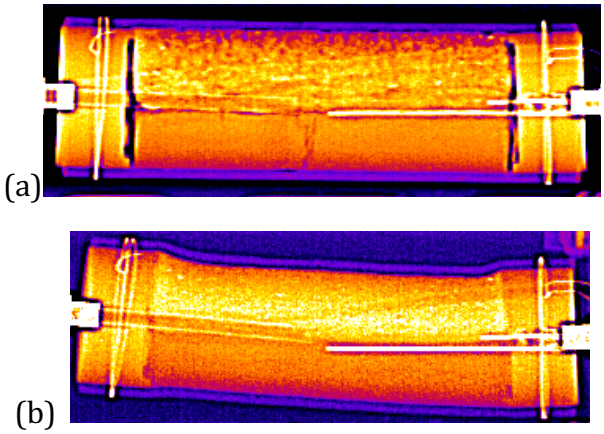

Figure 4.2. The packed mud/sand layered sample (a) Initial condition (b) After increasing the effective stress to 120 psi.

Slow depressurization

The pump volume variation during hydrate formation is plotted in Figure 4.3. During hydrate formation 53.71 mL (at 700 psi) of CH_4 was consumed to form hydrate. The consumed gas volume under the standard condition is 2592.90 mL.

The gray value variations in mud/sand layers after hydrate formation are shown in Figure 4.4(a). We found that the hydrate mainly formed in the sand layer, but it was not uniformly distributed. The increased gray value in mud layer may result from the compaction or from hydrate formation. In addition, the gray values in the initial state, gray value variation after hydrate and after water saturation were plotted in Figure 4.4(b).

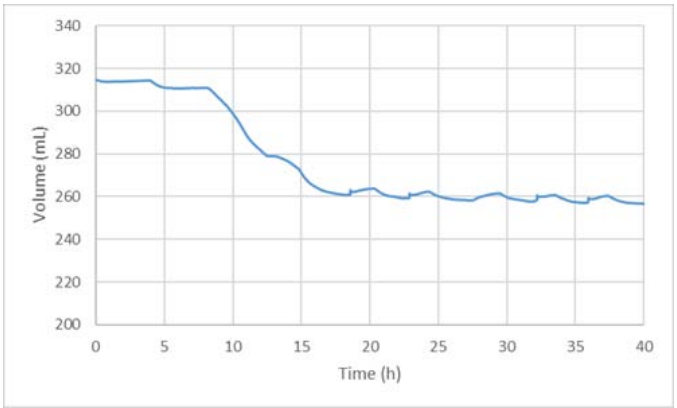

Figure 4.3. Pump volume variation during hydrate formation indicating methane consumption by hydrate formation.

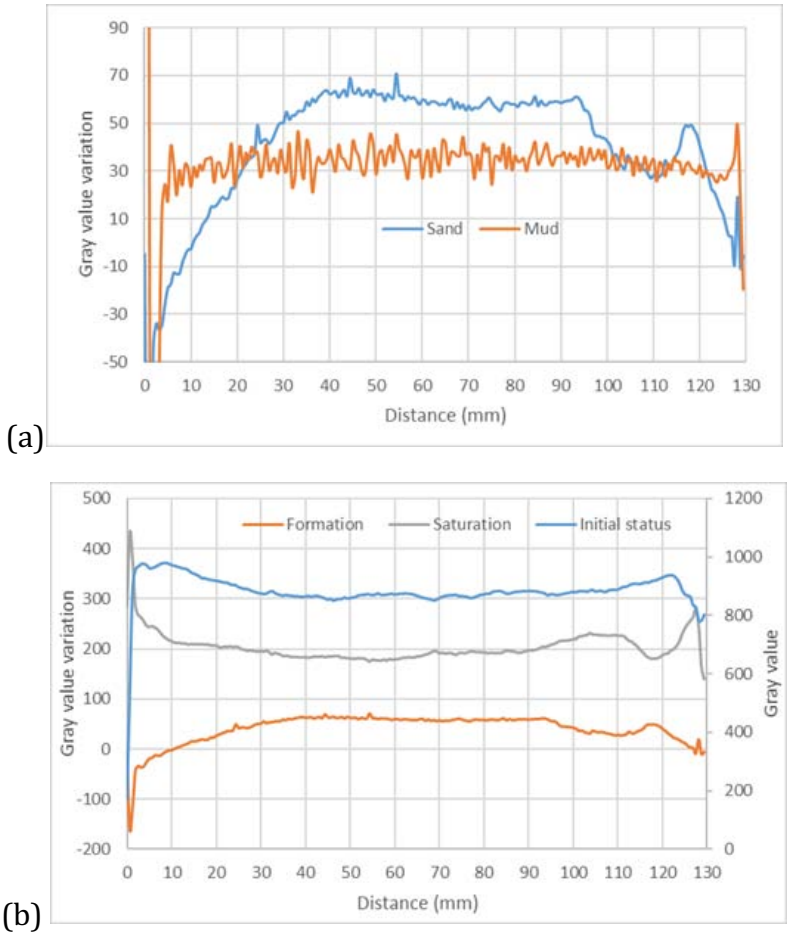

Figure 4.4. (a) comparison of X-ray CT gray value variation in mud and sand layers; (b) gray value variation in sand layer resulting from hydrate formation/water saturation.

After hydrate was formed, water was allowed to flow into and through the sample at rates of 0.5, 1 and 2 mL/min by setting the upstream pump to constant pressure and pulling water through the outlet into the downstream pump. Figure 4.5(a) shows the CT gray value variation in the sand layer after the water flow events. Although the results show some noise, they are generally negative indicating a decrease in density of the sample, which may have been caused by either loss of fine material, or loss of residual gas.

Subsequent to the water flow, the upstream pump was filled with CH_4 which was allowed to flow through the sample at a rate of 2 mL/min. The gray value variation after gas flow is plotted in Figure 4.5(b), the gray value changed significantly near the inlet (right side) and the variation decreased along the sample. There was no change observed in mud layer due to the limited permeability. In addition, hydrate formation was observed during gas flow consuming a gas volume of 955.38 mL under standard conditions. Figure 4.5(c) shows a cross section from a CT image

showing variation in density after gas flow, showing that the flow region was much broader near the inlet (lower part of image). In both gas and water flow operations, effluent was collected to determine if any movement of fine particles could be detected. In both cases, the turbidity of the effluent remained unchanged indicating no significant particle production.

Hydrate was dissociated by stepwise dropping of the pore pressure from 700 psi to 550 psi over 1.25 hrs (see Figure 4.6). The cumulative produced gas volume is plotted in Figure 4.7. The produced gas volume was 3356.90 mL (at STP), which was slightly lower than the consumed gas volume of 3548.28 mL, but represents a 95% recovery of CH_4. CH_4 left in the system (sample, tubing, etc) could account for approximately 100 mL, which would bring the mass balance to 98%.

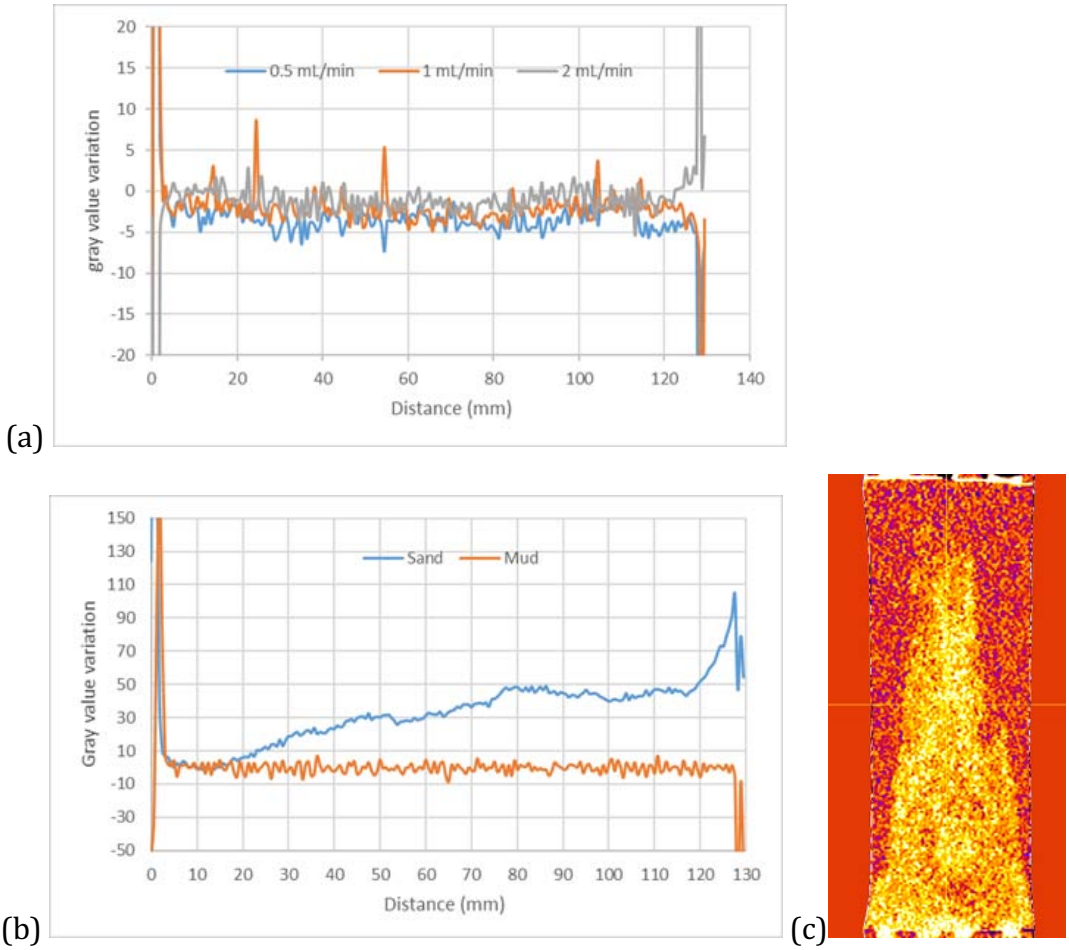

Figure 4.5. gray value variation in sand layer resulting from (a) water and (b) gas flowing, and (c) CT image variation after gas flow.

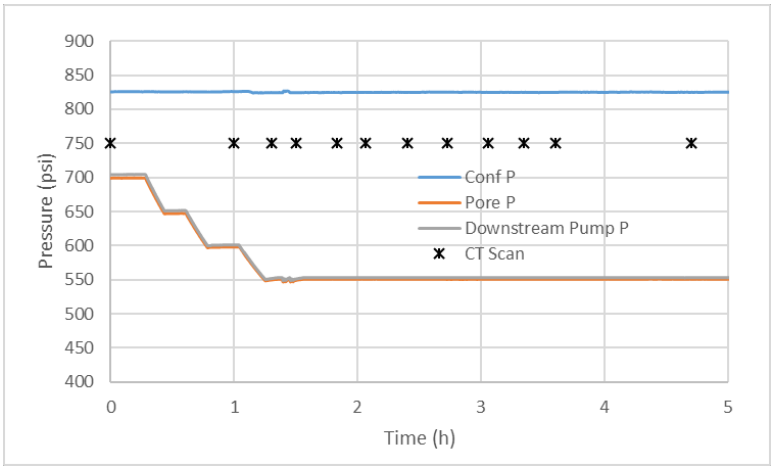

Figure 4.6. Pressure profile during hydrate dissociation and the CT scan.

(a)

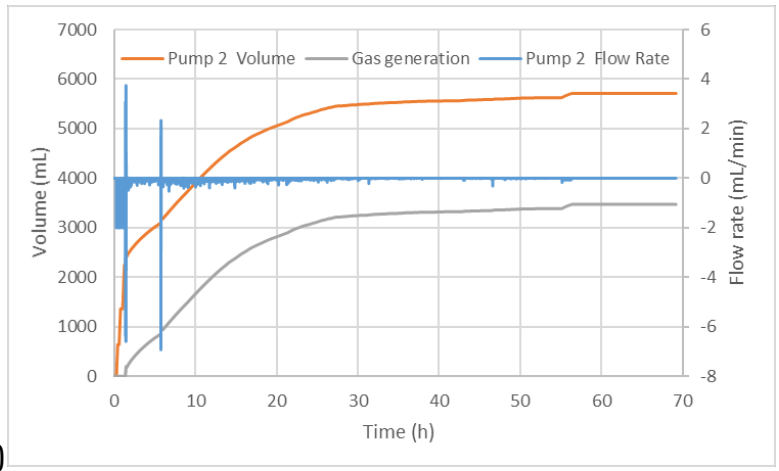

(b)

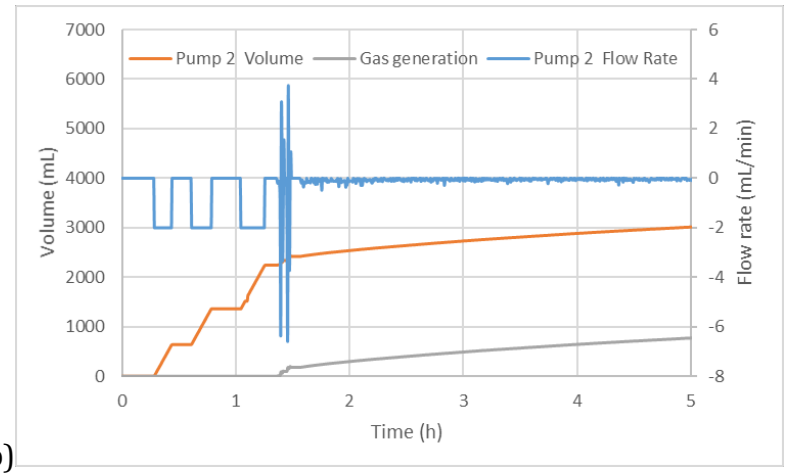

Figure 4.7. Cumulative produced gas volume.

Figure 4.8 shows the CT images during the hydrate dissociation process, in which the brighter color means more mass lost, indicating the hydrate dissociation. The

hydrate initially dissociated near the outlet (lower part of image), where free gas existed in the pore space. Figure 4.9 shows gray value variation in mud/sand layers along with the sample during hydrate dissociation process. The positive gray value means mass loss. As shown, hydrate mainly dissociated in the sand layer. But the gray value decreased in the mud layer, indicating a mass increase.

After dissociation, water was flowed through the sample (rate of 1.0 mL/min) and the results were shown in Figure 4.10. The top of the figure, 4.10(a) shows the difference in grey value after flow. The water mainly flowed through the sand layer. As shown in Figure 4.10(b), some sand particles moved out near the outlet (left side, darker section in the CT images). Figure 4.11 shows the variation in the number of pixels in each slice during hydrate dissociation process. As the scan number increases (as shown in the legend) dissociation is proceeding. Pixels represent cross sectional area of the sample, therefor results indicate that the sample became smaller in this plane with hydrate dissociation.

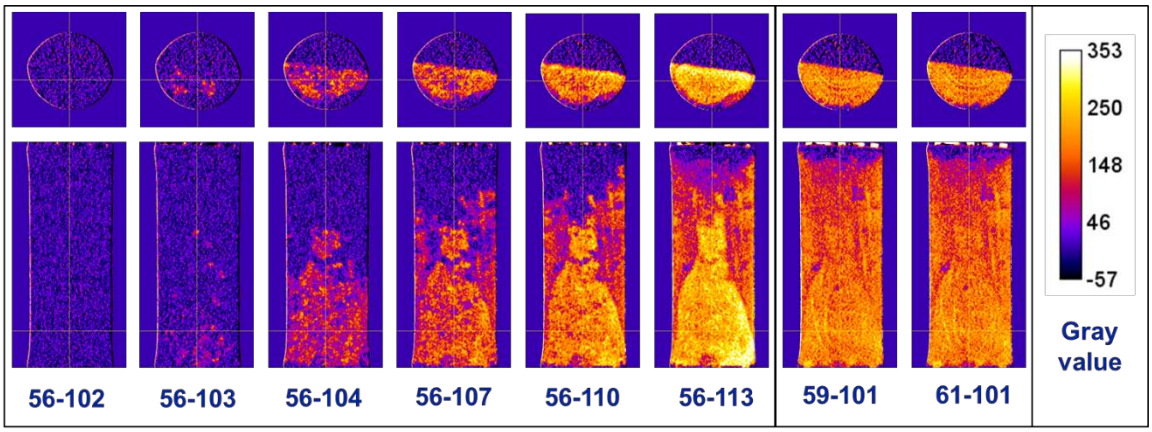

Figure 4.8. CT images during hydrate dissociation.

(a)

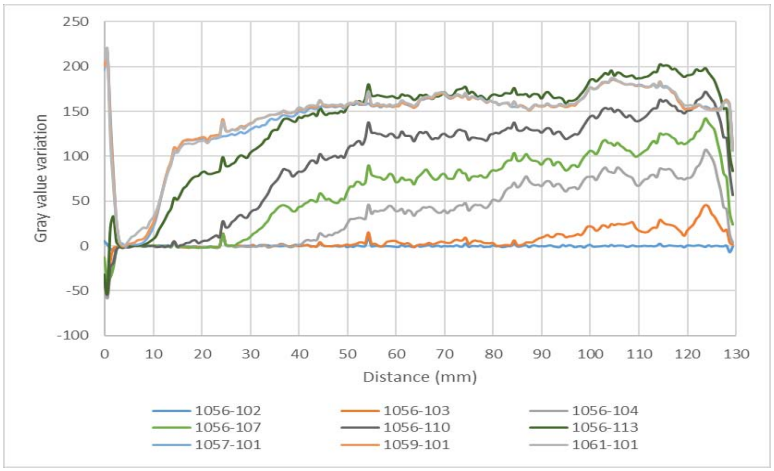

(b)

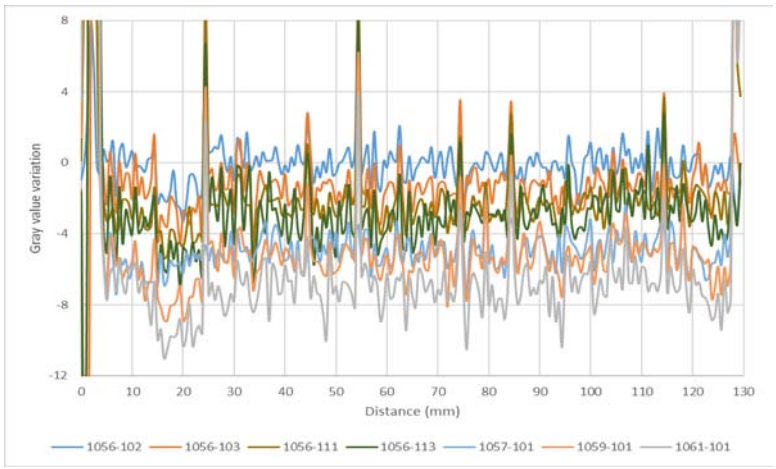

Figure 4.9. Gray value variation in (a) sand and (b) mud layers along with the sample during hydrate dissociation process.

(a)

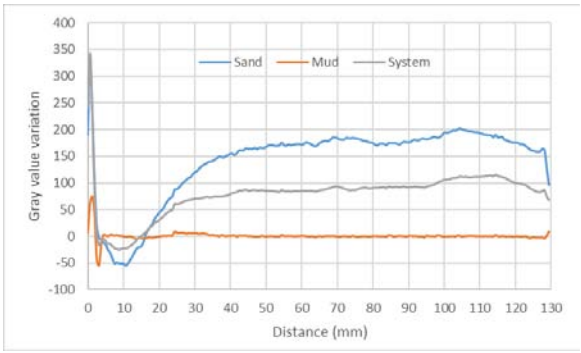

(b)

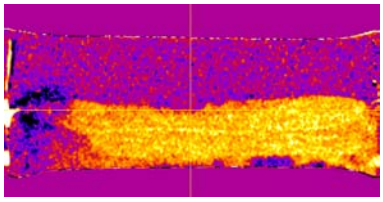

Figure 4.10. (a) gray value variation in layer sample resulting from water flow after hydrate dissociation in the mud layer, sand layer, and in the combined (mud + sand) system. (b) CT image of the increase in density (dissociated sample subtracted from water saturated dissociated sample) variation after water flow. Sand is on the bottom, mud on top. The darker color of the mud layer indicates little change in density while the brighter color of sand shows a greater change.

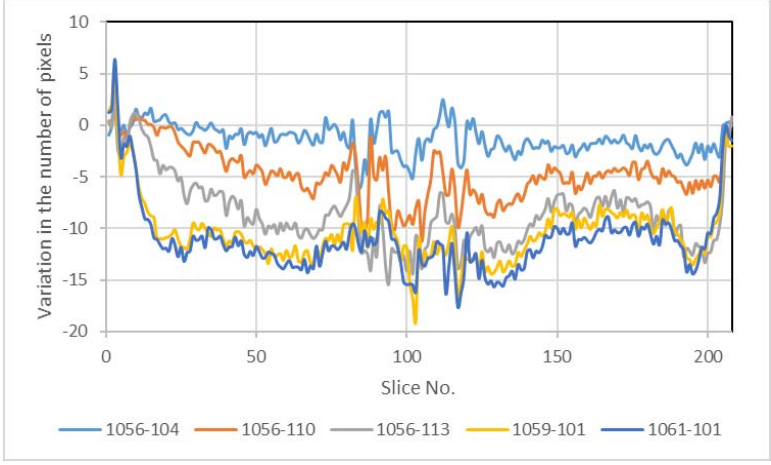

Figure 4.11. Variation in the number of pixels in each slice during the hydrate dissociation process. The number of pixels represent the cross sectional area of the hydrate sample. As hydrate was dissociated (dissociation indicated by increasing scan number), the sample area decreased.

Rapid Depressurization

The temperature and pressure profiles during the hydrate formation process are plotted in Figure 4.12. Pore pressure was maintained at 700 psi and the hydrate formed in about 28h based on the temperature variation. Due to a fluid leak, no quantitative data on amount of methane consumed during formation was possible. The reason for the pressure and temperature fluctuations at ~120h is due to water injection into the vessel. As with the slow depressurization test, the hydrate was saturated with water after formation. A CT image of the water-saturated hydrate-bearing sample is shown in Figure 4.13, showing a small decrease in density near the outlet.

Figure 4.19 summarizes the average gray value variation in the sand layer during the hydrate decomposition process. The average gray value variation increased as hydrate dissociated, which indicates a continuous mass loss.

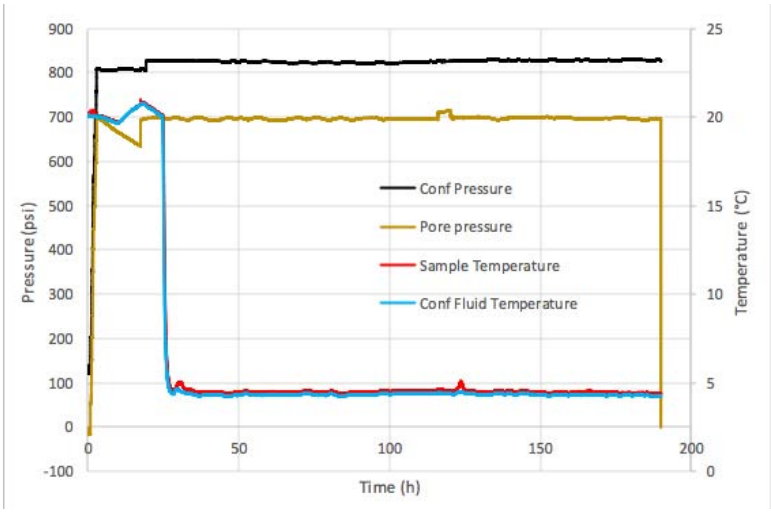

Figure 4.12. The temperature and pressure profiles during hydrate formation process. Top graph is the first 200 hrs, bottom half shows the first 40 hrs in more detail.

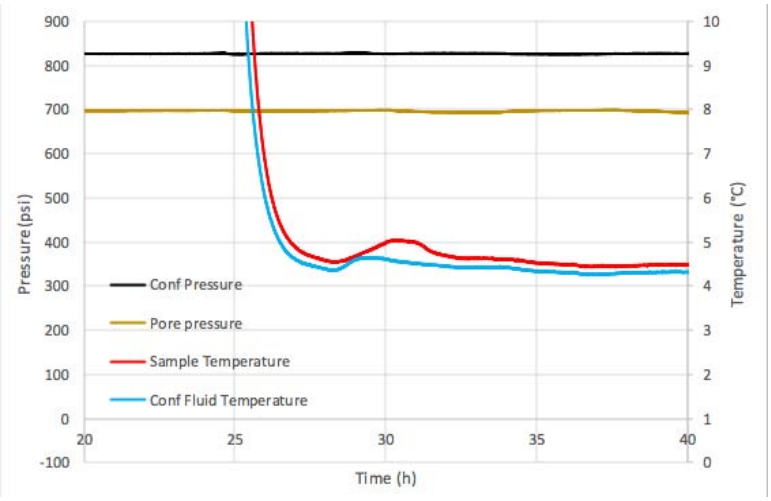

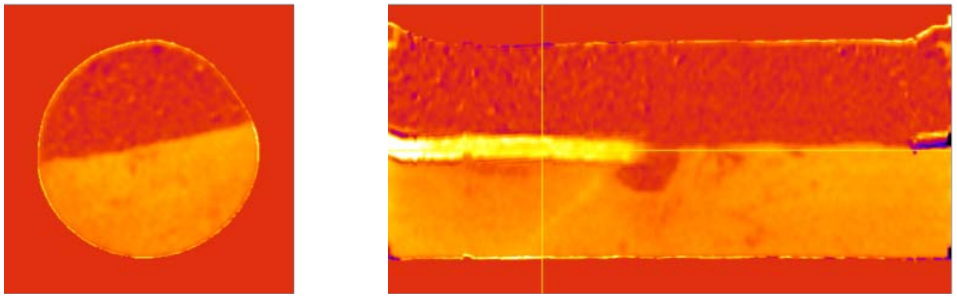

Figure 4.13. Gray value variation before and after water saturated. The darker color in the sand layer near the outlet mid-sample may indicate some movement of sand.

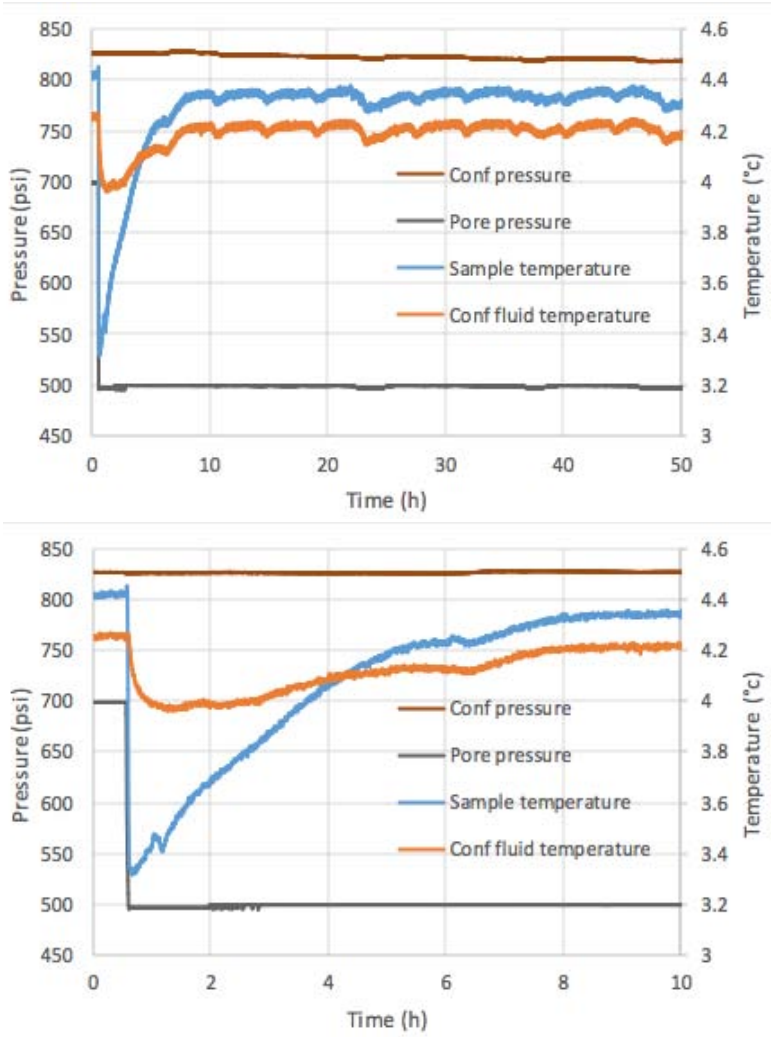

Figure 4.14. The temperature and pressure profiles during hydrate decomposition process – rapid depressurization. Top graph is the first 50 hrs, bottom is the same data showing the first 10 hr in greater detail.

Figure 4.14 shows the temperature and pressure profile during the hydrate dissociation process. Pore pressure was dropped rapidly (over 10 min) from 700 psi to 500 psi, after which the pore pressure and confining pressure were maintained at 500 psi and 820 psi, respectively, during the hydrate dissociation process. However, the temperature significantly decreased once the pore pressure decreased from 700 psi to 500 psi, and then increased to the initial values with the hydrate dissociation due to heat transfer from the ambient. The temperature decrease was due to 1) endothermic hydrate dissociation reaction and 2) Joule-Thomson cooling.

In Figure 4.15,the pressure-temperature curve is compared with the phase equilibrium curve proposed by Kamath (1987). The results show that the rapid depressurization induced hydrate dissociation can be mainly divided into three stages: 1) rapid pressure relief; 2) hydrate dissociation along the phase equilibrium

curve with the sensible heat of the reservoir supplying heat for the hydrate dissociation; and 3) the pressure drop to the selected gas production pressure, and ambient heat transfer drives the hydrate dissociation reaction.

The volume change of the pressurized methane gas, considered to be the cumulative gas production, is shown in Figure 4.16. The amount of produced methane gas is ~82.61 mL at 500 psi, which corresponds to 2892 mL at STP. Figure 4.17 shows the CT scanned images during the hydrate dissociation process, the brighter color means more mass lost, indicating the hydrate dissociation. The hydrate dissociation mainly occurred in the sand layer. This gas amount is less than the amount collected during the slow depressurization (3357 mL) but during the slow depressurization test additional hydrate formation was observed during methane flow through the sample. The amount recovered here is similar to the amount consumed during initial formation in the slow depressurization test (2593 mL).

In addition, the information in the CT images was extracted and illustrated in Figure 4.18. The results show that the gray value variations in the sand layer increased as the hydrate decomposed, however, those in the mud layer exhibited similar values. These results suggest that the hydrate mainly formed in the sand layer.

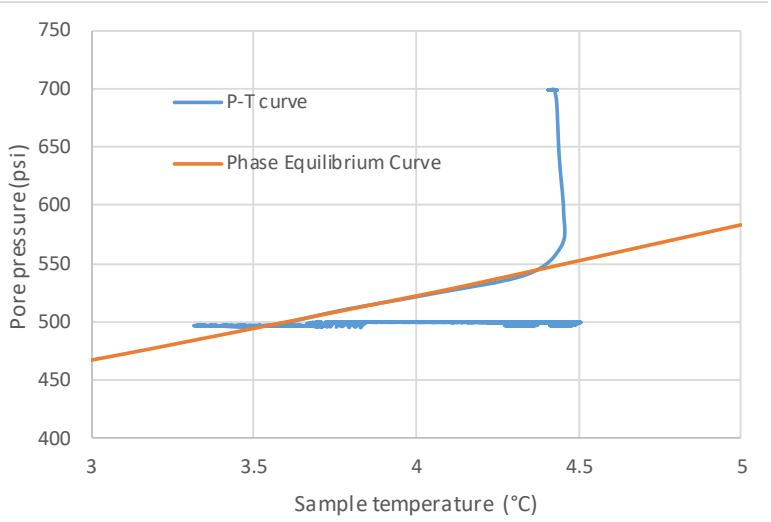

Figure 4.15. Variation in pore pressure with respect to the temperature during hydrate dissociation process, in relation to the phase equilibrium curve proposed by Kamath (1987).

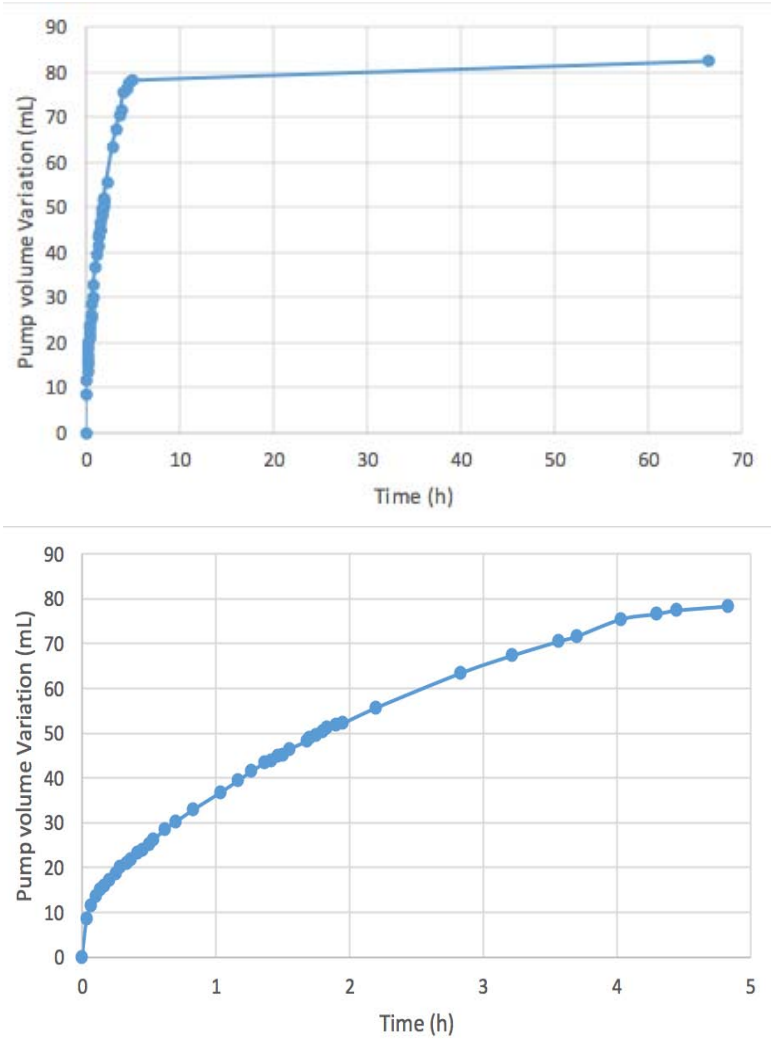

Figure 4.16. Volume change of the pressurized methane gas during gas production process.

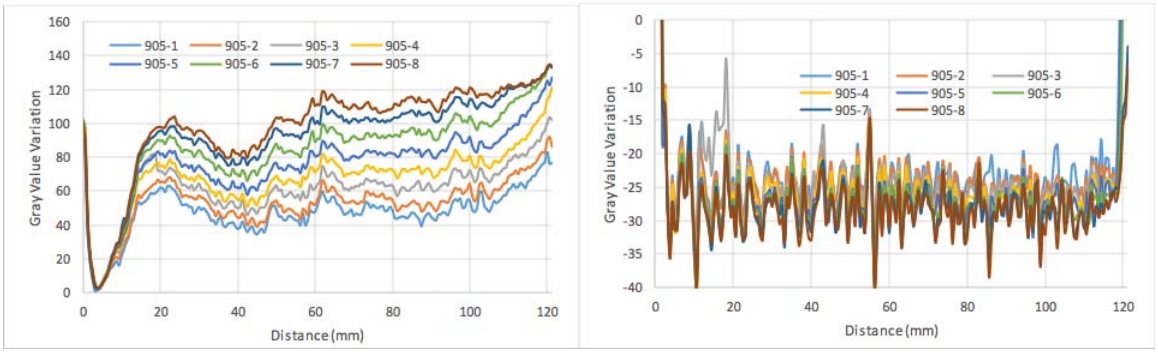

Figure 4.17. Gray value variation in the mud layer (left) and sand layer (right) along with the sample length.

(a) 38 min 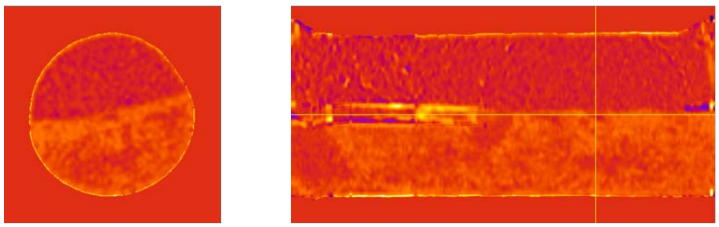

(b) 51 min 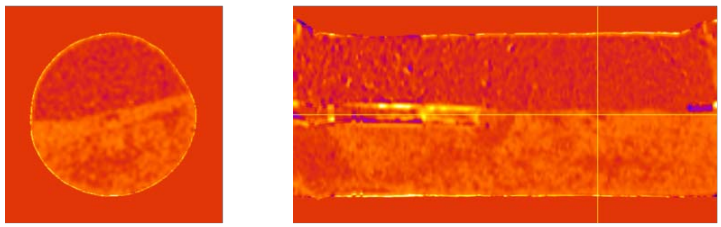

(c) 71 min 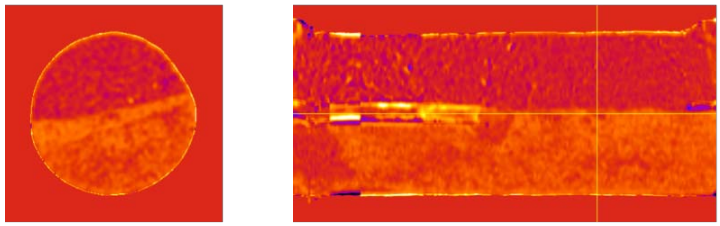

(d) 95 min 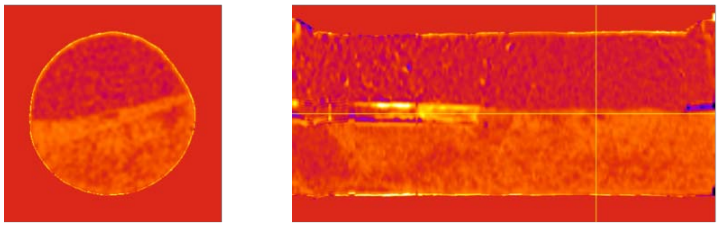

(e)128 min 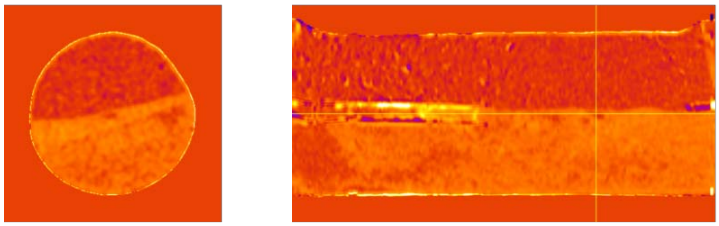

(f) 177 min 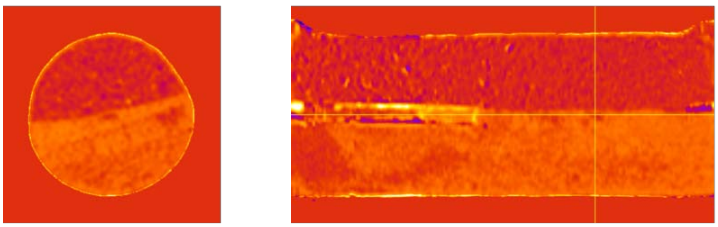

(g) 222 min 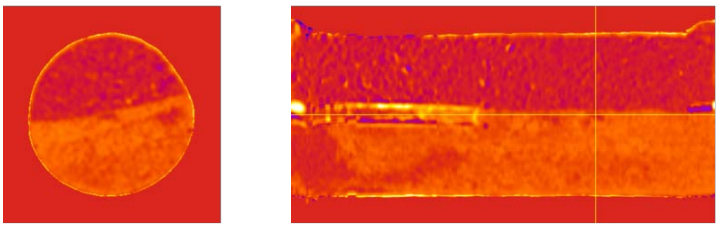

(h) 275 min 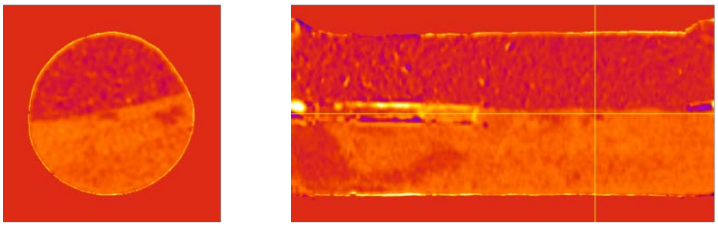

Figure 4.18. CT scanned images during hydrate dissociation process. The brighter color means more mass lost, indicating the hydrate dissociation from the lower sand layer.

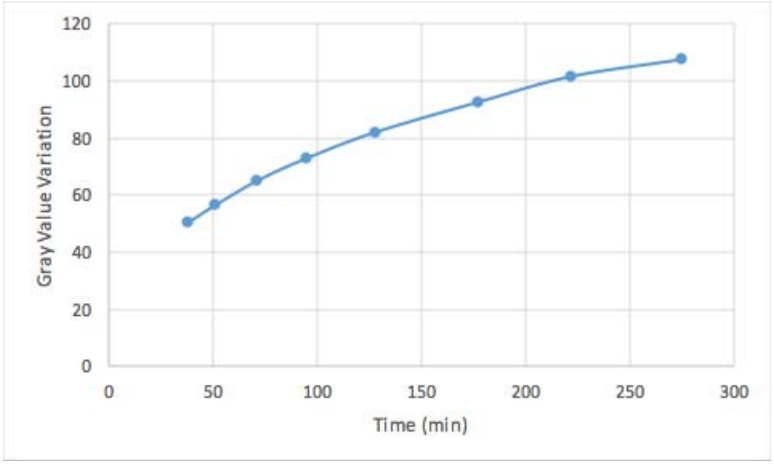

Figure 4.19. Average gray value variation in the sand layer indicating hydrate dissociation.

Task 5: Mechanical and chemical behavior of diatomaceous medium and filtration behavior of sand

Sharon Borglin, Bin Wang, Tim Kneafsey

Introduction

This task requested that realistic effective stress changes be applied to samples with sand and diatomaceous earth (DE) to investigate compaction of DE and possible movement of fines. In addition, clay composition in the basin was to be reviewed and laboratory tests using real sediments to investigate the degree of swelling were to be performed. Finally, using real or simulated media (sediments) the magnitude the effect of fines production was assessed.

A survey of known literature on sediments in the Ulleung basin showed mostly silt and clay layers with an overall mean particle size ~10 μm, and diatoms sizes on the order of 50 μm (Kim et al, 2013; Yun et al, 2011). Specification on the clay type were uncertain, so a non-swelling clay, Kaolin, was used for this task. Naturally occurring (real sediments) were not available for testing. The artificially constructed sediments were a mixture of silt (Sigma) (200g), kaolinite (50g) diatomaceous earth (2.5g) (Sigma) and water (50g). Images taken of the diatomaceous earth show both intact and broken structures (See Figure 5.1).

To investigate movement of diatomaceous earth in sand, laboratory tests were performed by placing diatomaceous medium (medium particle size 50 μm) in discrete regions of a packed sand column (medium particle size 150 μm). A band of barium sulfate (5 μm) was also placed in the sample. Barium sulfate is not water soluble and is often used as a contrast agent, and it was used here as an example of a fine particles easily located by X-ray CT.

The outlet of the column was screened to prevent movement of sand. The sample was placed in a pressure vessel and an effective stress of 120 psi was applied. Changes in effective stress (120 to 300 psi) were applied followed by flows of water and gas through the column with flow rates up to 20 ml/min and the sample was imaged by periodic CT imaging to image movement of the finer particles through the sand. The diatomaceous earth (DE) had a lower density than the sand and the barium sulfate higher density.

Despite several liters of flow through the system, the bands of DE and barium sulfate appeared to remain intact and no significant visual movement fines migration was detected. Figure 5.2 shows the sample (flow bottom to top) of the original sample, sample after water flow, and sample after gas flow. Figure 5.3 plots the grey value variations along with the axis of sediments. Grey value is related to density, and changes would indicate movement of material. The grey value of barium sulfate is the biggest, followed by F110 sand, and DE smallest. In this figure, water flow was from the right to the left. As shown, the grey value in the upstream side of $BaSO_4$

layer decreased slightly and increased on the downstream edge, which may indicate some minor movement. The same figure shows small movement of DE and some changes at the inlet and outlet.

More detailed analysis is shown in Figure 5.4 which displays histogram distributions of grey value in the $BaSO_4$ layer for each slice upstream and downstream of the $BaSO_4$ band. The grey value of $BaSO_4$ in the center of the band was above the limit for the scanner as samples with grey values larger than 3000 indicate an insufficient flux of X-rays. Individual images show distribution of grey values before (red) and after (blue) flow of water. The direction of water flow in the series of figures is from top to bottom and left to right, i.e. a higher slice number means a shorter distance from the entrance. Slice 193 located immediately upstream of the $BaSO_4$ layer and slice 182 immediately downstream of the $BaSO_4$ layer. In this figure if the $BaSO_4$ fines moved due to the water flow, then the intensity downstream from the band would increase, and the intensity of the band upstream would decrease. There is some evidence of loss of signal in slices 192-186, and some increase in signal in slice 185, but any change is minimal.

This experiment was repeated with similar bands of DE and $BaSO_4$ with the modification that the BaSO4 layer was mixed to a level that allowed penetration of x-rays. Again, in this sample minimal if any movement of either material through sand was observed with an effective stress of 120 psi. Up to 1400 mL of water was passed through the sample with no significant changes to the density or configuration of the sample.

Some experiments were performed with sand samples (F110 sand, 150 μm mean particle size) when the outlet of the sample was unscreened. Figure 5.5 shows the sample deformation resulting from effective stress changes (100 – 400 psi), gas flow (up to 20 mL/min), and water flow (up to 20 mL/min) in the unscreened system. The results indicated that samples collapsed near the outlet as a result of sand leaving the system. The flow of water was most detrimental to the stability of the sample.

In the layered samples described in Task 4 the mud layer contained a mixture of silt (16 μm mean particle size), kaolinite (4 μm mean particle size), diatomaceous medium (50 μm mean particle size), and barite (4.5 μm mean particle size), and the sand layer was made from F110 sand. In these samples migration of sand was prevented by an aluminum screen placed over the outlet. This screen has a mesh size larger than the medium diameter of sand (0.011 in, 280 μm). After hydrate formed, flows of both water and methane through the sample were applied to observe any effect to the sample due to migration of sediment or fines. Mechanical differences such as density changes and sample size due to fines migration were observed by CT. Some increase in density of the mud layer (top half) due

compaction of the sample was observed, but this was difficult to quantify due to the presence of the barite (Figure 5.6).

To further assess fine particle or sand movement, a sand trap was placed downstream from the outlet during the hydrate tests in layered systems. Visual inspections and turbidity measurements were made on effluent samples collected in this trap. Turbidity values were barely above the background water measurements, and overall the sediment showed no appreciable accumulation of material. Particle size analysis was done on samples from the mud and sand layers from before and after hydrate formation (see Table 5.1) which showed minor changes in overall composition. However, in the CT scan cross section, some movement of sand through the screen located at the outlet can be seen, and physical inspection of the endcap shows that some sand did migrate through the screen (Figure 5.7).

Conclusion

Overall, despite water and gas flows, hydrate dissociation and effective stress changes, the movement of sand and fine materials was not significant in our experimental systems if the outlet of the sample was physically constrained by a plug or screen.

Table 5.1. Particle size distribution of the samples before and after hydrate formation. Changes in particle size distribution show minor changes in the fines (less than 50 um) in both the sand and the mud layer.

Size range	Pre sand	Post sand	Pre mud	Post mud
Less than 2 um	0	0	6.84%	6.08%
Between 2 and 50 um	0.78%	0.03%	59.41%	53.73%
Between 50-100 um	17.12%	18.51%	15.7%	16.79%
Between 100-250 um	74.27%	74.18%	15.9%	17.61%
Between 250 and 500 um	7.84%	7.28%	2.16%	5.76%

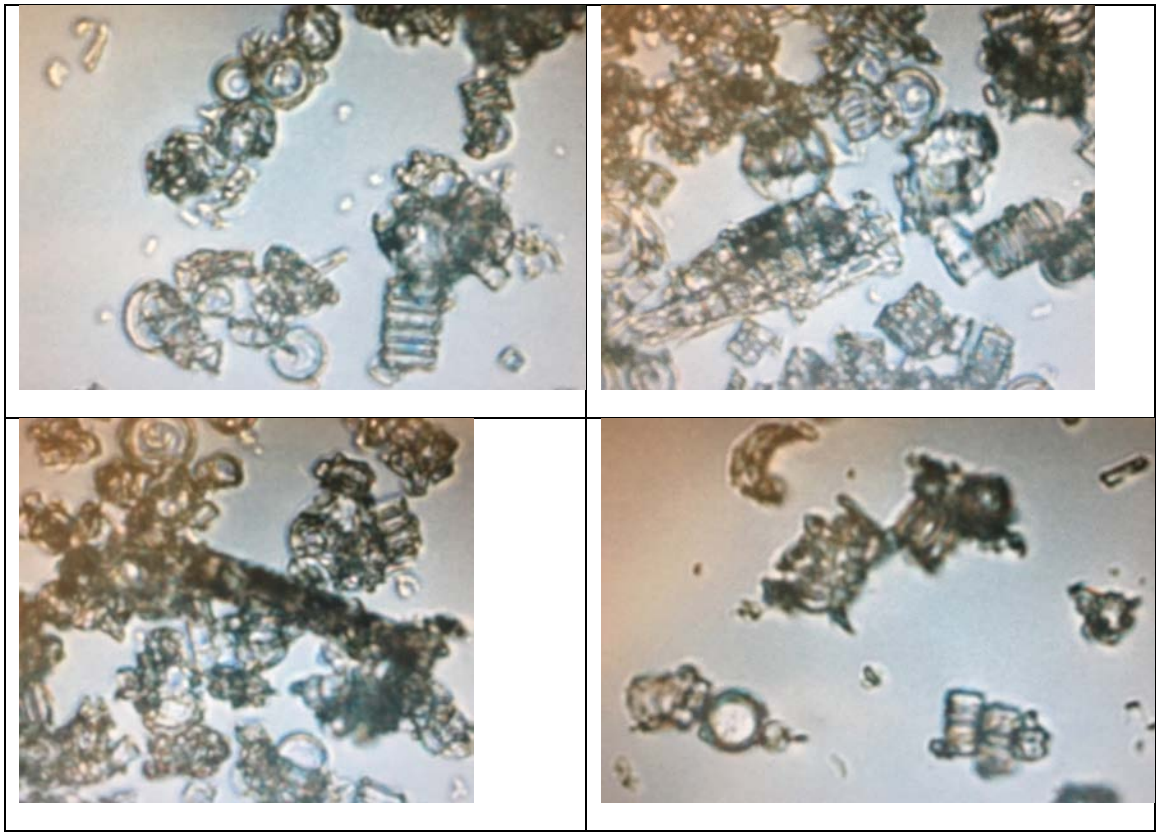

Figure 5.1. Microscopic images of diatomaceous earth.

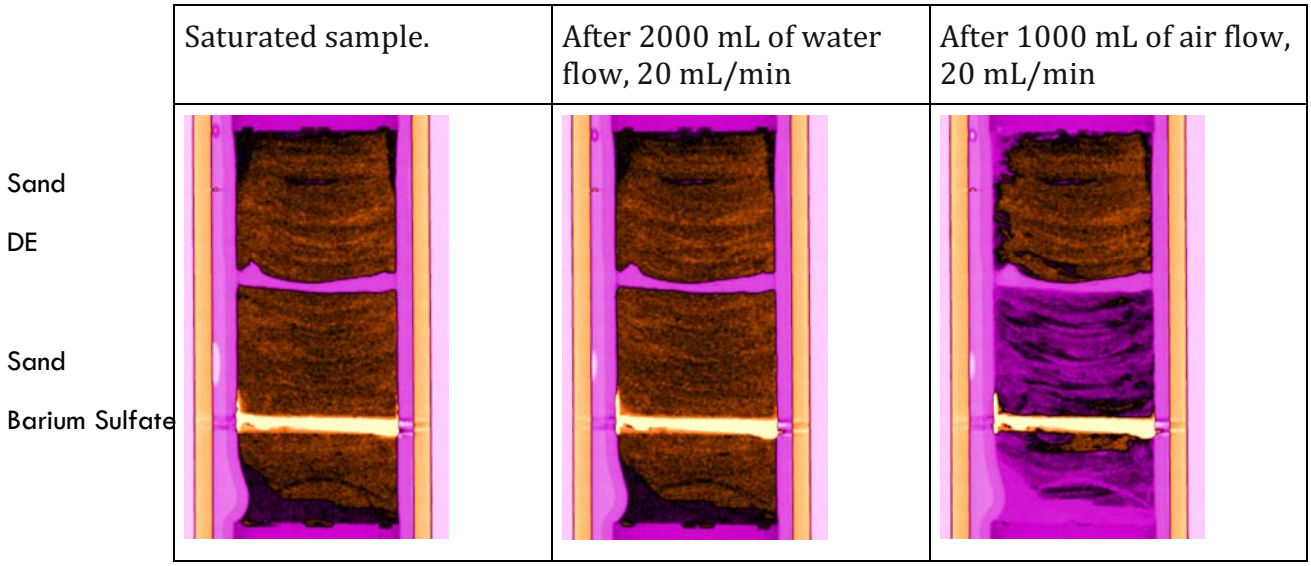

Figure 5.2. Cross section of sand sample containing a layer of diatomaceous earth (DE) and barium sulfate. Flow was from the bottom to the top of the sample.

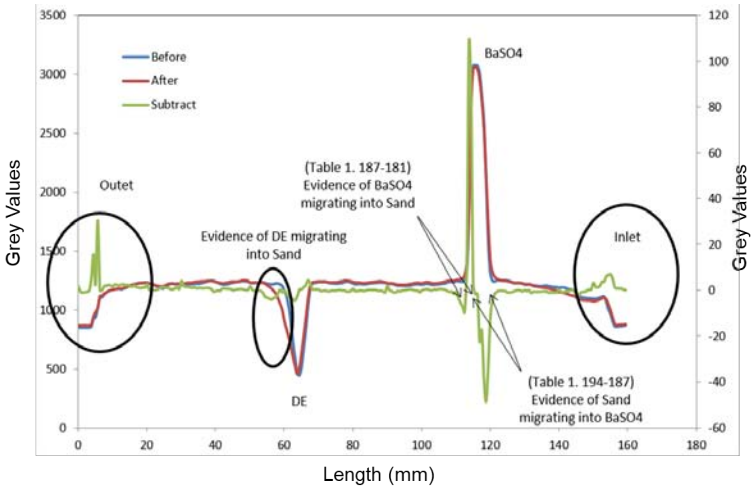

Figure 5.3. grey value variations along with the water flow direction

Slice 193

Slice 182

flow

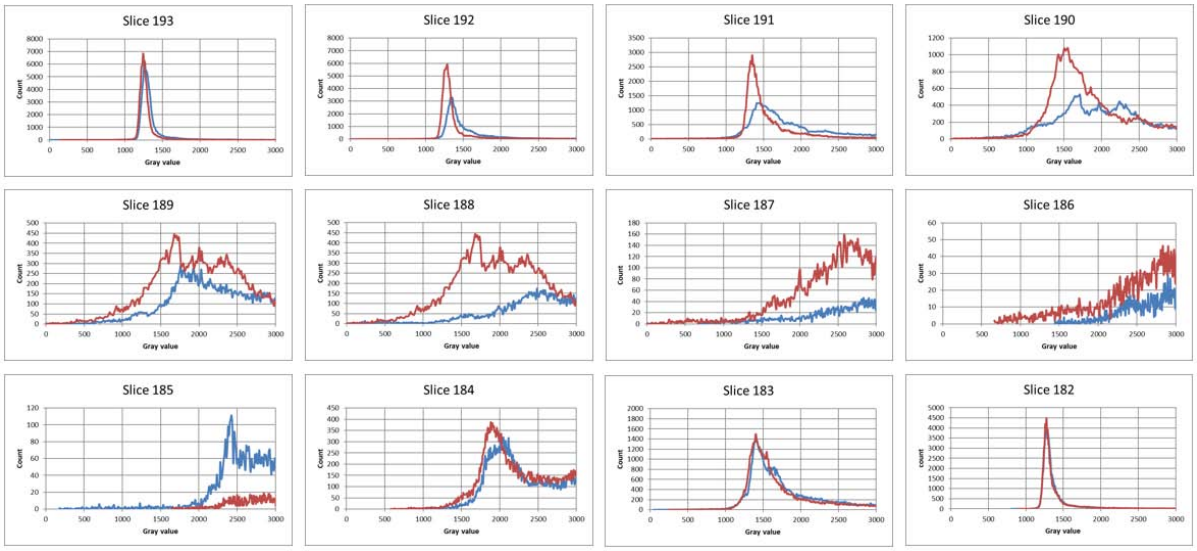

Figure 5.4. $BaSO_4$ layer histogram distribution. The red and blue lines indicate before and after water flow respectively.

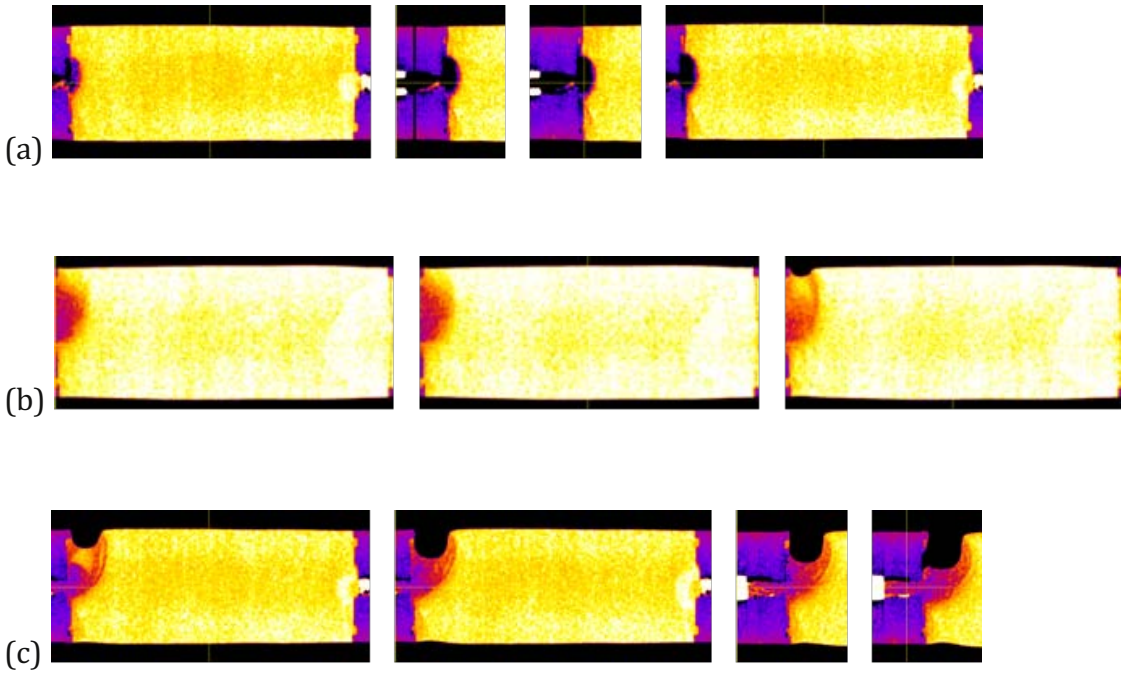

Figure 5.5. Deformation of F110 sand as a result of (a) increasing effective stress (b) gas flow and (c) water flow. Outlet was unplugged to allow sand flow.

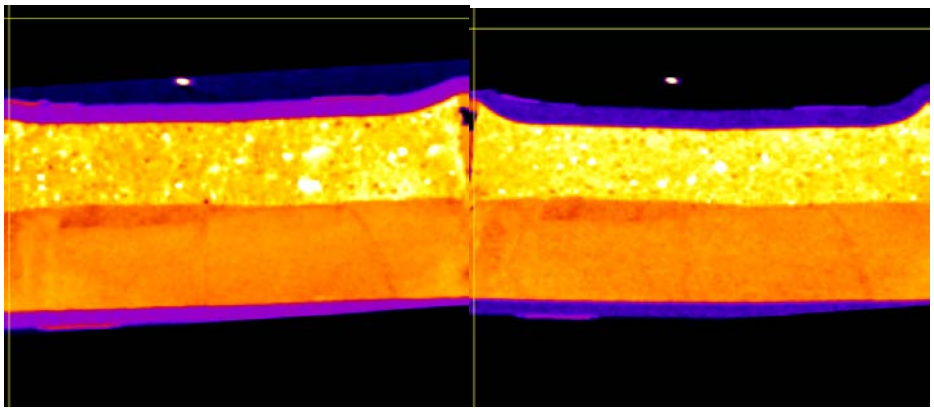

Figure 5.6. X-ray CT images of layered mud (top layer) and sand (bottom layer). (a) Sample before hydrate formation and water/methane flows (b)sample after water and methane flows, and after hydrate dissociation.

Figure 5.7. Evidence for fine particles migration (end cap).

References

Barree, R. D., & Conway, M. W. (2004, January 1). Beyond Beta Factors: A Complete Model for Darcy, Forchheimer, and Trans-Forchheimer Flow in Porous Media. Society of Petroleum Engineers. doi:10.2118/89325-MS

Kamath, V.A., G.D. Holder, Dissociation Heat Transfer Characteristics of Methane Hydrates, AIChE J. 33 (1987), 347-350.

Kim, H., Cho, G., Lee, J.,Kim, S. (2013). Geotechnical and geophysical properties of deep marine fine-grained sediments recovered during the second Ulleung Basin Gas Hydrate expedition, East Sea, Korea. Marine and Petroleum Geology. 47. 56-65. 10.1016/j.marpetgeo.2013.05.009.

Lee, C., Byun, Y. Lee, J. (2015). Geotechnical and Geoacoustic Properties of Volcanic Soil in Ulleung Island, East Sea of Korea. Marine Georesources & Geotechnology. 34. 150725145132000. 10.1080/1064119X.2015.1070387.

Malek, K. and M.O. Coppens, Knudsen self- and Fickian diffusion in rough nanoporous media. *Journal of Chemical Physics*, 2003. **119**(5): 2801-2811.

Oyama, H., Abe, S., Yoshida, T., Sato, T., Nagao, J., Tenma, N.,Narita, H. (2016). Experimental study of mud erosion at the interface of an artificial sand-mud alternate layer. Journal of Natural Gas Science and Engineering. 34. 10.1016/j.jngse.2016.07.067.

Shi, H., Holmes, J.A., Durlofsky, L.J., Aziz, K., Diaz, L., Alkaya, B., Oddie, G., (2005) "Drift-Flux Modeling of Two-Phase Flow in Wellbores." SPE J. **10**(1): 24-33.

Yun, T. S., C. Lee, J.-S. Lee, J. J. Bahk, and J. C. Santamarina (2011), A pressure core based characterization of hydrate-bearing sediments in the Ulleung Basin, Sea of Japan (East Sea), *J. Geophys. Res.*, 116, B02204, doi: 10.1029/2010JB007468.

LBNL-KIGAM Collaboration in the Investigation of the Gas Production Potential of Hydrate Deposits in the Korean East Sea

A proposal submitted to the

Korea Institute of Geoscience and Mineral Resources (KIGAM)

and

National Energy Technology Laboratory (NETL)

by

Lawrence Berkeley National Laboratory (LBNL)

Energy Geosciences Division

1 Cyclotron Rd.

Berkeley, California 94720

USA

Principal Investigator: Timothy J. Kneafsey

Co-PI: George J. Moridis

Co-PI: Matthew T. Reagan

May 27, 2016

PROJECT DESCRIPTION

I. Introduction

This proposal discusses two groups of tasks having the goal of improving understanding of the future production of methane from hydrate deposits in the Ulleung Basin (UB). The first group of tasks are numerical, to be performed using TOUGH+HYDRATE and other codes developed at Lawrence Berkeley National Laboratory. The second group of tasks are experimental, to be performed in laboratories at Lawrence Berkeley National Laboratory. All tasks are to be performed in collaboration with or with inputs from KIGAM.

Numerical Simulations
Lawrence Berkeley National Laboratory (LBNL) is a world leader in hydrate research and the developer of the TOUGH+HYDRATE code [*Moridis et al*., 2008] for the simulation of fluid and heat flow and transport in hydrate-bearing sediments. TOUGH+HYDRATE (T+H) was designed to model non-isothermal CH_4 release, phase behavior and flow under conditions typical of CH_4-hydrate deposits (i.e., in the permafrost and in deep ocean sediments) by solving the coupled equations of mass and heat balance, and is among the most advanced hydrate codes in the world. T+H is currently involved in practically every hydrate-related research project in the world. Because of its very large computational requirements of the T+H code, a parallel version, pT+H, [*Zhang et al*., 2008] has been developed and is used by several research organizations.

The T+H code has been coupled with the FLAC3D geomechanical code [*Rutqvist and Moridis,* 2009*; Rutqvist et al.,* 2009; *Kim et al*., 2012a] to investigate coupled flow, thermal and geomechanical processes for the analysis of the mechanical stability of the HBS and of the wellbore assemblies in hydrate deposits under production, and to determine the envelope of geomechanically safe operations. More recently, T+H was coupled with ROCMECH [*Kim et al*., 2012b], a powerful geomechanics code developed at LBNL, which has the added benefit of parallelization (a problem with FLAC3D).

A multi-year collaboration between KIGAM and LBNL has resulted in extensive research into the potential for production from gas hydrates for several UB reservoirs. To continue this collaborative work, the objectives of this proposed study are:

(a) Leverage recent LBNL work in the simulation of shale gas/shale oil systems to add non-Darcy flow, inertial effects, turbulent, and other physics of flow in very high-*k* and low-*k* porous media to T+H/pT+H. This will allow more

realistic modeling of the near-wellbore zone in the thinly bedded mud/sand systems found in UB gas hydrate systems.

(b) To improve the reliability of the prediction of production behavior and wellbore stability in UB gas hydrate systems. For this, we will incorporate the most complete geomechanical modeling capabilities into the coupled pT+H-ROCMECH simulator, implement a detailed, realistic representation of the wellbore itself, and further investigate the effect of hydrate dissociation on the reservoir and the stability of the well assembly.

(c) Via (a)-(c), create capabilities to be used in future collaborative work between KIGAM and LBNL—in the planning of upcoming UB expeditions and in the design of future field tests.

(d) To participate in a possible DOE-led code comparison study for geomechanical simulators and coupled flow-geomechanical (T-H-M) codes.

The results of this work informs KIGAM's Production Technology Study, which will design optimal production schemes and evaluate the safety and stability of boreholes/wells and the stability of the reservoir during production. As such it can help determine locations best suited to the upcoming 3rd UBGH Drilling Expedition and the future production field test.

Experimental Studies

Sediments containing methane hydrate in the UB have been described to be high plasticity clayey silts with a clay fraction less than 10-20% and a sand fraction less than 10% and having permeabilities on the order of 10^{-3} to 10^{-1} mD, [*Kwon, Lee et al.* 2011], organic clay of medium to high plasticity or diatomaceous silty clay [*Yun, Lee et al.* 2011], and high-plasticity silts with specific surface S_a ~21 to 31 m^2/g consisting of microfossils with some illite, kaolinite, and chlorite. Diatoms determine particle size distribution and cause both a dual porosity microstructure, and high initial void ratio [*Lee et al.* 2011]. Other descriptions include methane hydrate contained in ~ meter-scale thick sand layers between layers of sediments as described above.

For gas production from hydrate, issues associated with these stratigraphies include permeable muds limiting the effectiveness of the seal, fines migration with fluids removal, reduction in sediment strength with hydrate dissociation and gas migration, and the possible lack of gas-flow pathways. Strategies to extract and collect gas from nodule and vein-filling hydrate configurations are under consideration and addressed in the numerical simulations, but no ideal strategy has been developed. Approaching the lower-hanging fruit of producing gas from hydrate-bearing sand between clay and sand-containing plastic silts is considered here.

Hydrate production using depressurization is considered here because it is more likely to have a greater reach from a well than inhibitor or thermal techniques. Two configurations are considered – vertical wells and multi-stage horizontal wells (Figure 1). In the vertical well geometry, a well is drilled into and finished in the hydrate-bearing layer. Fluid extraction (or introduction) is through the well, and a simple conceptual model of flow is radial. Fluid flow to or from the well will have the greatest effect in the immediate vicinity of the well, thus any damage there from mechanical failure of the medium or well will affect future production. In the multi-stage horizontal well, a horizontal well would be drilled and finished with a lumber of stages in the hydrate-bearing zone, probably towards the top to take advantage of gas buoyancy. Fluid production through the first stage (at the far end) would be performed initially. If mechanical failure of the well or sediment in that vicinity occurred, that stage would be shut off and production from the second stage implemented. This would continue until production reached stage "n" at which time another horizontal multi-stage lateral would be completed in another direction and the process repeated. If the hydrate-bearing layer is thin, this method arranges the well to be closer to a larger quantity of the hydrate resource, and allows for mechanical failure without total system failure. An alternative method for producing gas from alternating mud-sand sediment layers with a vertical well is to produce gas at multiple stages from deeper levels of the vertical well. Similarly to the horizontal well case, the section of the well is abandoned as the reservoir is depleted and the sediments subside. To avoid shearing of the casing, production schedules from multiple wells need to be coordinated carefully, with monitoring of the reservoir compaction and seafloor subsidence. This type of reservoir management has been proposed and implemented in oil fields with shale layers which causes well shear failure due to slip at sedimentary boundaries induced by subsidence. System optimization would be required including understanding of the geometries, mechanical and hydrological characteristics of the deposit, and economics of operation.

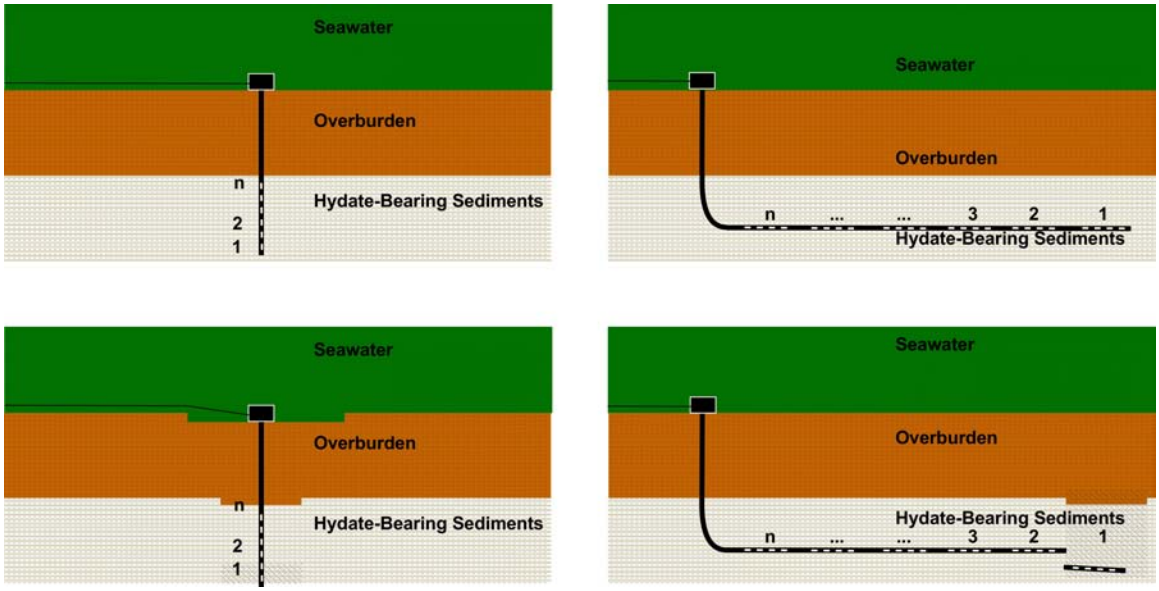

Figure 1. (Left) multi-stage vertical well geometry, (Right) multi-stage horizontal well geometry, (Bottom) Multi-stage well eliminating end stage.

Regardless of the well geometry, a number of issues need to be addressed: mechanical and hydrological behavior of the reservoir materials under producing conditions.

II. Project Tasks

The proposed project is a continuation of ongoing LBNL-KIGAM collaborative studies on the subject of gas production from hydrates. In the ensuing discussion, references to "effort" are to indicate the time needed by LBNL scientists to accomplish the tasks described later in this section. Numerical simulation studies are described in Tasks 1-3, and Laboratory studies are described in Tasks 4 and 5. Regarding some of the geomechanical numerical simulation work in Task 2, LBNL will coordinate with the research team of Dr. Kim at Texas A&M University for better coupling algorithm for numerical stability and accuracy, and LBNL will also share and discuss the geomechanical simulation results with Dr. Kim, as required.

Numerical Simulation Tasks

Task 1: Enhanced flow simulation capabilities for the simulation of complex mud/silt/sand hydrate-bearing systems

Subtask 1.1: Non-Darcy capabilities for T+H codes
Duration: 6 months, i.e., from 10/1/2016 to 3/31/2017
Budget: $25K (LBNL portion - funded by US DOE)

Previous studies have demonstrated the technical feasibility of gas production from hydrate deposits in general, and the feasibility of production from the reservoirs identified in the UBGH1 and UBGH2 drilling expeditions. The systems modeled to date involved sandy production zones layered between mud/silt barriers, and have be represented by traditional Darcy's Law treatment of flow in porous media. Current work at KIGAM involves review of UBGH1 and UBGH2 data (sedimentology and geochemical analysis, geophysical inversion and seismic modeling) and geological model development to better understand and characterize these reservoirs. To model such deposits may require more advanced simulation capabilities that include the complex behavior of low effective permeability fractured mud/clay systems, low-permeability/high-saturation hydrate inclusions, and transport through high-permeability pathways. We propose to expand the capabilities of the T+H/pT+H codes through the additional of several non-Darcy flow effects:

(1) Implementation of non-Darcy flow effects for high-permeability media (fractured hydrates, vertical pathways in fractured muds/silts), including:
   (a) The Drift-Flux model [Shi et al., 2005; Livescu et al., 2010] to allow the simulation of fluid flow and accurate phase segregation in high-permeability pathways, i.e., wellbore flow and flow in pathways created by dissociation of hydrates.
   (b) Forchheimer flow; for the representation of high-velocity turbulent flow through high-*k* media, particularly in hydrate-free regions near the wellbore.

(2) Implementation of non-Darcy flow effects for very low-*k* media (muds, high hydrate saturation, other low-effective permeability), including:
   (a) Knudsen diffusion; for systems where the gas mean-free path is comparable to the pore diameter.
   (b) Klinkenberg effects; to correctly represent gas flow in low-permeability/tight media.

   The inclusion of such inertial effects is deemed important because the effective permeabilities of hydrate-bearing media (HBM) are often at a level comparable to that of ultra-tight media (such as shale gas reservoirs), and because they are a possible explanation of the higher than expected permeabilities observed in HBM under production.

Note that, although the duration of this project is short and the budget is limited, the new simulation capabilities will leverage recent NETL-funded work on coupled T-H-M simulation of shale gas and shale oil systems. The capabilities needed to represent mud/clay systems are similar to those currently implemented in the TOUGH+RealGasBrine and TOUGH+MultiComponentMultiphase simulators, and these features will be adapted to T+H/pT+H.

Subtask 1.2: Simulation of complex mud/silt/sand deposits
Duration: 6 months, i.e., from 12/1/2016 to 6/30/2017
Budget: $25K (LBNL portion - funded by US DOE)

Using the capabilities developed in Subtask 1.1 and geological models developed in collaboration with KIGAM, this subtask will evaluate via numerical simulation the production behavior the mud/silt/sand discovered in the previous UBGH1 & 2 expeditions. Given the limited budget and duration, a limited set of "schematic" systems will be examined to determine the effect of the additional modeled processes listed in Subtask 1.1, and to determine the potential productivity of such systems. If these results prove to be promising, future collaborative work may be proposed to further evaluate the importance of these effects.

This task will also leverage the results of the laboratory work proposed by other KIGAM collaborators (Kneafsey, Seol) and incorporate any new information gained about effective permeability and flow through sand/mud/silt systems. Such laboratory data, if suitable, will be incorporated as options (describing new relationships between k_{eff} and S_H for mud/silt systems) into the T+H code and will be used to validate available flow models and re-analyze the results of earlier tests.

Task 2: Enhanced geomechanical capabilities for the predictive simulation of potential UBGH field test sites

Duration: 6 months, i.e., from 5/16/2017 to 11/31/2017
Budget: $80K (funded by KIGAM)

Recent collaborative studies between KIGAM and LBNL have demonstrated the importance of considering geomechanics during production from gas hydrates, and how geomechanical stability limitations may inhibit production from an otherwise promising hydrate deposit. The most recent UBGH2 simulations, performed in 3D with coupled geomechanics (using T+H-ROCMECH) indicate that subsidence of the overburden and potential uplift of the underburden may jeopardize wellbore stability for systems with certain geomechanical properties.

Discussions with KIGAM indicate that wellbore stability is of particular concern in field-test design. In this task, we proposed to implement a realistic representation of the wellbore to better understand the hazards created during production from UB reservoirs. The simulations in this task are to be conducted using T+H coupled to the ROCMECH code (Kim et al., 2012). In addition, this task will leverage other research being conducted at LBNL and we will consider the use of new, more advanced geomechanical simulators that are currently under development if such methods are deemed more suitable to solving this problem.

With the full-wellbore treatment in place for the UBGH 2-6 case, we will assess well stability and the possibility of cement failure during production for various production scenarios using 3D parallel coupled flow-geomechanical simulation. We will also re-evaluate the geomechanical stability of the formation and the productivity of the reservoir by considering plasticity and large-deformation geomechanics. This work will also include an effort to validate coupled TOUGH+ROCMECH vs. the pre-existing experimental data.

Because of the very demanding computational requirements of this work, it will not be possible to analyze the geomechanical behavior of more than one deposit. To leverage previous work, we propose to limit the simulations to the UBGH2-6 reference case developed during the previous round of LBNL-KIGAM collaborator studies.

Task 3: Project Management, Communication, Reporting and Technology Transfer

Duration: 20 months, i.e., from 10/1/2016 to 5/30/2018
Budget: $5K (LBNL portion – funded by US DOE)

As in any collaborative project, significant communications and interactions are necessary between LBNL and KIGAM. These include telephone discussions, telephone- and video-conferencing, e-mail communications, in addition to review meetings (at the LBNL campus and, possibly, at the KIGAM headquarters in Korea) for joint studies and for project progress review. Reporting requirements include (a) the LBNL submission of quarterly progress reports to the KIGAM team by e-mail and (b) a final project report by 6/1/2017, in addition to (c) notifications when significant milestones are reached. Technology transfer includes the publication of papers and scientific presentations at professional meetings. Technology transfer may also include training of KIGAM scientists in the use of the enhanced LBNL T-H-M codes (possibly conducted at LBNL facilities in Berkeley, after a commensurate increase in the project budget).

Laboratory Study Tasks
Task 4: Gas production from a sand layer in a sand/mud layered system

Duration: 12 months, i.e., from 5/16/2017 to 4/13/2018
Budget: $70K (LBNL portion – funded by KIGAM)

The essential question is: Can gas be effectively produced from the layered sand/mud system?

Proposed study:

A layered sand/mud system will be constructed in a laboratory pressure vessel using real (from Korea) or simulated media. It is envisioned that a 2-layer system be initially investigated because that contains the essence of the problem. One of the layers will be composed of silts and diatoms, the other of sand also containing some silts and diatoms (Figure 2). Methane hydrate will be formed in the sample (primarily in the sand using the excess gas method), and the sample will then be

saturated with water. Upon water saturation, the sample will be flowed initially under conditions where gas hydrate is stable, examining any fines migration using X-ray CT and possibly an optical method in the flowing fluid. After either equilibration or a sufficient time, the system will be 1. slowly, or 2. rapidly depressurized to mimic a 1. smaller or 2. larger change in effective stress representing distance from the well. The excess stress will be carefully controlled and the fluids, solids, and gas production will be observed using a variety of techniques.

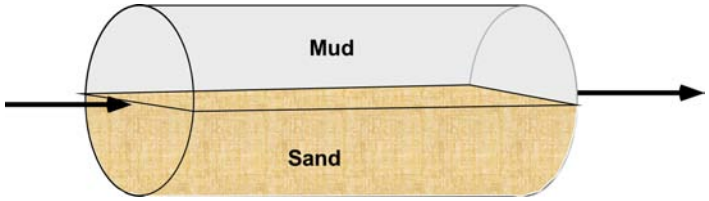

Figure 2. Gas production test schematic.

Following each test, both sand and mud fractions will be carefully sampled for further analysis by KIGAM working with the USGS to evaluate the transport of fines in both media.

Task 5: Mechanical and chemical behavior of diatomaceous medium and filtration behavior of sand

Duration: 12 months, i.e., from 10/1/2016 to 8/30/2017
Budget: $70K (LBNL portion – funded by US DOE)

Mechanical behavior: The literature cited here indicates that the diatomaceous nature of the medium must be considered, as the diatoms are likely to break under reasonable stress [*Kwon et al.* 2011, *Lee et al.* 2011, *Yun et al.* 2011] causing compaction, and production of smaller fines that may be transported.

Chemical behavior: The effect of freshening was brought up by *Kwon et al.* [2011]. Although it was not possible to differentiate the effect of medium alteration by gas generation and freshening, this was used to partially explain higher compression indices upon hydrate dissociation.

Filtration: A pumped well will draw fluid through the sand, and that fluid may carry fines. Production of gas in the hydrate may stir up the medium (typically sand)

which is under low effective stress, or gas bubbles may mechanically scrub particles from sand grains, allowing them to be transported.

Proposed study:

a. Using numerical simulation of realistic UB conditions either from the literature or from KIGAM, a set of realistic effective stress changes related to production will be determined. These will be compared to the literature for diatomaceous porous medium behavior to estimate the extent of this issue. Note that for either well geometry, conditions near the well are critical. For a horizontal well in sand, the change in effective stress on the diatomaceous medium will be mitigated by the presence of the sand layer. Laboratory tests will be performed to examine compaction of real (supplied by Korea) or simulated diatomaceous porous media, and the production and transport of created fines. As diatomaceous earth is a filter material, transport may not be an issue, however this transport during consolidation particularly where possible diatom breakage could occur has not been investigated.
b. The composition of clays in the analyses reviewed does not indicate a strong swelling fraction. The initial part of the study will involve reviewing clay composition from literature and reports and determining the magnitude of potential swelling. Laboratory tests using real preserved sediments are desired to examine the magnitude of the swelling effect. In these tests, the medium will be appropriately compacted into in an oedometric (~zero-lateral strain) cell, and saturated with water having a desired salinity (e.g. seawater). The sample will be loaded compressively, and then fresh water supplied while monitoring swelling.
c. Using realistic conditions from numerical modeling or supplied from KIGAM, the potential for fines migration will be considered. Using real (supplied by Korea) or simulated media, the magnitude of this problem and how it could affect gas production from hydrate will be investigated using simplified setups.

V. **Deliverables**

The deliverables of this project include:

(1) A minimum of one paper on the topic of T-H-M modeling of production and wellbore stability in UB gas hydrate reservoirs, submitted for publication in a peer-reviewed journal.
(2) Samples from tests performed for analysis (e.g. Task 4) by KIGAM.
(3) A report on the numerical simulations to KIGAM by 10/31/2017.
(4) Short mid-term progress report to KIGAM by 10/31/17.
(5) Final report including all 5 tasks by May 30, 2018.

VI. **Project Location, Duration and Budget**

The project will last from October 1, 2016 to May 30, 2018. Most of the work will be conducted at the LBNL campus in Berkeley, California.

The total requested budget for the project is **$275K**. Of the **$275K**, **$150K will be provided by KIGAM**; the remaining **$125K** will be provided by the U.S. Department of Energy (DOE) as their contribution to the U.S.-Korea collaborative studies on gas production from hydrates. The KIGAM-funded portion includes **$30K** funding within Task 2 for Dr. Kim at Texas A&M University. The effort requirements described in this proposal correspond to the entire project, and not only to the part funded by KIGAM.

References:

Kim, J., Moridis, G.J., Yang, D., Rutqvist, J. (2012a). "Numerical Studies on Two-Way Coupled Fluid Flow and Geomechanics in Hydrate Deposits." SPE J. June 2012, 485-501.

Kim, J., Moridis, G.J., Rutqvist, J. (2012b). "Coupled flow and geomechanical analysis for gas production in the Prudhoe Bay Unit L-106 well Unit C gas hydrate deposit in Alaska." J. Pet. Sci. Eng. **92-93**, 143-157.

Kwon, T.-H., K.-R. Lee, G.-C. Cho and J. Y. Lee (2011). "Geotechnical properties of deep oceanic sediments recovered from the hydrate occurrence regions in the Ulleung Basin, East Sea, offshore Korea." Marine and Petroleum Geology **28**(10): 1870-1883.

Lee, C., T. S. Yun, J.-S. Lee, J. J. Bahk and J. C. Santamarina (2011). "Geotechnical characterization of marine sediments in the Ulleung Basin, East Sea." Engineering Geology **117**(1–2): 151-158.

Livescu, S., Durlofsky, L.J., Aziz, K., Ginestra, J.C. (2010). "A fully coupled thermal multiphase wellbore flow model for use in reservoir simulation." J. Pet. Sci. Eng. **71**: 138-146.

Moridis, G.J., Kowalsky, M.B., Pruess, K., (2008). "TOUGHþHYDRATE v1.0 User's Manual: A Code for the Simulation of System Behavior in Hydrate-Bearing Geologic Media." Report LBNL-00149E, Lawrence Berkeley National Laboratory, Berkeley, CA.

Rutqvist J., Moridis G.J. (2009). "Numerical Studies on the Geomechanical Stability of Hydrate-Bearing Sediments." SPE J. **14**: 267-282. SPE-126129. (2009).

Rutqvist, J., Moridis, G.J., Grover, T., Collett, T. (2009). "Geomechanical response of permafrost-associated hydrate deposits to depressurization-induced gas production." J. PEt. Sci. Eng. **67**: 1-12.

Shi, H., Holmes, J.A., Durlofsky, L.J., Aziz, K., Diaz, L., Alkaya, B., Oddie, G., (2005) "Drift-Flux Modeling of Two-Phase Flow in Wellbores." SPE J. **10**(1): 24-33.

Yun, T. S., C. Lee, J.-S. Lee, J. J. Bahk and J. C. Santamarina (2011). "A pressure core based characterization of hydrate-bearing sediments in the Ulleung Basin, Sea of Japan (East Sea)." Journal of Geophysical Research: Solid Earth **116**(B2): n/a-n/a.

Zhang, K., Moridis, G.J. (2008). "A domain decomposition approach for large-scale simulations of coupled processes in hydrate-bearing geologic media." Proc. 6th International Conference on Gas Hydrates, July 6–10. Vancouver, British Columbia, Canada.

National Energy Technology Laboratory

626 Cochrans Mill Road

P.O. Box 10940

Pittsburgh, PA 15236-0940

3610 Collins Ferry Road

P.O. Box 880

Morgantown, WV 26507-0880

1450 Queen Avenue SW
Albany, OR 97321-2198

Arctic Energy Office

420 L Street, Suite 305

Anchorage, AK 99501

Visit the NETL website at:

www.netl.doe.gov

Customer Service Line:

1-800-553-7681